Energy Accumulation and Emanation at Low Latitudes. Part II: Nonlinear Response to Strong Episodic Equatorial Forcing

HAI-RU CHANG AND PETER J. WEBSTER

Department of Meteorology, The Pennsylvania State University, University Park, Pennsylvania

(Manuscript received 24 October 1989, in final form 21 May 1990)

ABSTRACT

A fully nonlinear model is used to reexamine the impact of a zonally varying basic state on the propagation characteristics of latitudinally equatorially trapped modes. Linear studies have shown that such modes are longitudinally trapped in regions of negative stretching deformation of the equatorial time-mean zonal flow (i.e., where $U_x < 0$) forming "accumulation" regions of wave action flux. Furthermore, the accumulation regions tend to act as local emanation regions to the extratropics. These physical communications between the tropics and extratropics are referred to as *fast teleconnections* due to their rapidity (periods of days to weeks) compared to the much slower climatological differences in the mean states such as occur between El Niño and La Niña. The latter form of communication between low and high latitudes, which is induced by very low frequency SST changes, is referred to as a *slow teleconnection.*

It is generally found that accumulation and emanation regions are present in the nonlinear regime with much the same character as with the linear model. The similarity exists even when realistic forcing functions are used with amplitudes and temporal and spatial characteristics that correspond to impulsive convection in the western Pacific Ocean. A description of the convection is given. A diagnosis of the linear and nonlinear results shows that, in the tropics, the linear advection by the mean flow plays a dominant role and probably is the reason for the great similarity of the linear and nonlinear tropical atmosphere. However, there are some differences between the linear and nonlinear results. Nonlinear waves appear to propagate more rapidly through the maximum westerlies along the equator and with less difficulty than linear waves. The differences that do occur arise from the nonlinear changes in the tropical mass field, especially in the accumulation zone. Differences between linear and nonlinear responses in the midlatitude response to equatorial forcing appear to reflect changes in the tropics. Nonlinear maxima occur poleward of the region of tropical westerlies but only after accumulation has occurred along the equator.

The results of the study are used to discuss the problem of why there is considerable similarity between simple linear models and more sophisticated nonlinear models. Such similarity would probably explain why the NMC and the NEPRF global models exhibit phase locked responses in the middle latitudes to imposed and impulsive tropical forcing. The role of fast teleconnections in the longer term general circulation of the atmosphere is discussed, especially during El Niño and La Niña. Whereas an aggregate role for the fast teleconnections in producing very slowly evolving climate features remains obscure, it does appear that the accumulation-emanation theory may infer different routings for transient communications between the tropics and higher latitudes and vice versa depending upon the state of the basic flow.

1. Introduction

In a previous paper, Webster and Chang (1988, hereafter referred to as WC) demonstrated that the anomalous perturbation kinetic energy (PKE) maxima located in the upper tropospheric westerlies of the tropical mean flow could be explained, at least in part, by the control of the longitudinal stretching deformation of the equatorial time-mean zonal flow field (i.e., U_x) along the equator on the propagation characteristics of equatorially trapped modes. The WC hypothesis thus added a second mechanism that could explain the anomalous PKE in the nonconvective regions in the tropics. The first by Webster and Holton (1982), discussed the role of the propagation of extratropical disturbances into the tropics through the westerlies that span the upper troposphere between the two extratropical regions. Webster and Holton referred to the equatorial westerlies as the "westerly duct." WC emphasize that the two theories are not mutually exclusive.

In essence, WC were proposing a two time scale theory of tropical motions. The lower frequency flow is determined by the large asymmetries, longitudinal and latitudinal, in the sea surface temperature and the subsequent gradients in heating. Through the longitudinal component of the forcing, asymmetries in the zonal wind occur along the equator (e.g., Webster 1972) that are sufficiently strong to produce regions of mean upper

Corresponding author address: Prof. Peter Webster, Department of Meteorology, 503 Walker Building, The Pennsylvania State University, University Park, PA 16802.

tropospheric westerlies. Such regions are then suitable for the propagation of active extratropical transients into the tropics or through the tropics to the other hemisphere. (See Webster 1983 for a review of the influence of middle latitude events on the tropical circulation.)

a. The linear wave accumulation-emanation theory

Regions of anomalous PKE have been identified observationally by Murakami and Unninayer (1972), Arkin and Webster (1985), and, more recently, by Webster and Yang (1989). In the WC theory, waves with a longitudinal group speed component along the equator, presumably excited by the convective activity in the regions of upper tropospheric easterlies (see section 2), may possess zeros in their Doppler-shifted group speed (C_{gd}) in the region of negative stretching deformation of the equatorial time-mean zonal flow; i.e., where $U_x < 0$.

The theory that explains the accumulation of energy for an equatorially trapped mode emerges from rather simple considerations. Consider a wave of frequency ω propagating through a time invariant basic flow (or, at least, varying at a much longer frequency than the transient wave) that varies only in longitude such that $U = U(x)$. For such waves, the Doppler-shifted frequency ω_d ($=\omega - kU$) must be invariant along a ray path. Thus, if U changes along a ray then k, the longitudinal wavenumber, must change. The rate of change along a ray will be determined by the mode and the change of U in space. For an equatorial Rossby wave, WC show that the rate of change of k along a ray is given by

$$\frac{dk}{dt} = \frac{\partial k}{\partial t} + \left(U + \frac{\partial \omega}{\partial k}\right)\frac{\partial \omega}{\partial x} = -k\frac{dU}{dx}. \qquad (1)$$

Thus, if $U_x < 0$, a propagating mode must decrease its scale (i.e., k larger) to conserve its Doppler-shifted frequency. Conversely, if $U_x > 0$, the scale must increase (k smaller). As the group speed of Rossby modes is a strong function of k, the Doppler-shifted group speed also changes as a function of k. WC show that for the observed values of U and U_x, the Doppler-shifted group speed of westward propagating modes (i.e., the longer Rossby modes) goes to zero to the east of the maximum westerlies along the equator. Recently, Webster et al. (1989) have shown that modes with initially eastward Doppler-shifted group speeds (i.e., the shorter modes) will also be trapped in the tropical westerly regions.[1] This heuristic argument is supported by the consideration of the wave action density of equatorially trapped modes. For a slowly varying basic state, WC show that the wave energy density, ϵ, changes as

$$\frac{\partial \epsilon}{\partial t} + C_{gd}\frac{\partial \epsilon}{\partial x} = -\epsilon\frac{dU}{dx} \qquad (2)$$

where $\epsilon = \rho g h^2/2$ if h is the perturbation height of a shallow fluid. Equation (2) shows that regions of negative stretching deformation are convergent regions of wave energy density. If the stretching deformation is positive, the region is divergent.

Zhang and Webster (1989) have shown that the character of an equatorially trapped mode changes rapidly as a function of the sign of the basic state. Figure 1a (from Zhang and Webster 1989, Fig. 6) illustrates this property of equatorially trapped Rossby waves by showing the perturbation zonal wind structure for the

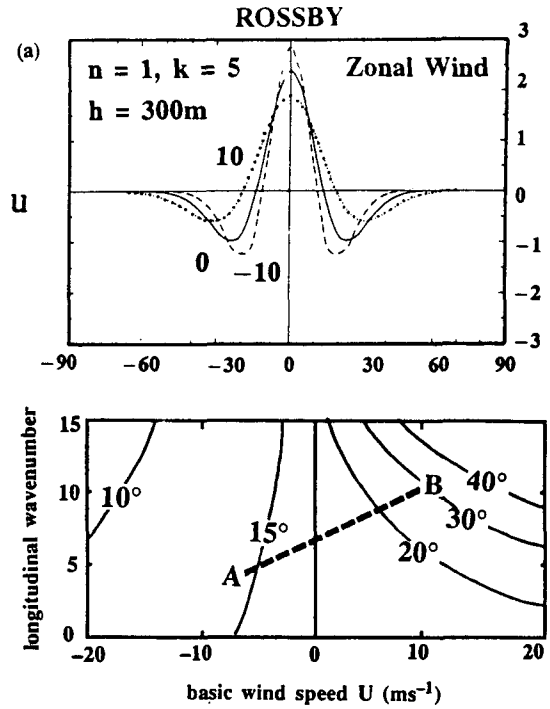

FIG. 1. (a) The perturbation zonal wind structure for the $n = 1$, $k = 5$ mode for basic states with mean zonal speeds of 10, 0, and -10 m s^{-1}. Note that the turning latitude of the mode is significantly more poleward for the westerly basic state than for the easterly basic state. From Zhang and Webster (1989). (b) Contours of the turning latitudes of the $n = 1$ mode as a function of longitudinal wavenumber and the basic zonal wind, U (m s^{-1}). The dashed line indicates the variation of turning latitude and scale of a mode propagating along the equator from the easterlies (point A) to the westerlies (point B). From Zhang and Webster (1989), and Webster et al. (1989) (see footnote 1).

[1] Webster et al. (1989), have shown that the eastward and westward propagations are comprised of the long Rossby wave packet, which propagates westward, and a short scale Rossby wave packet, which propagates eastward. Both sets of modes will accumulate in the negative stretching deformation region for the observed parameter range. They refer to the upper-tropospheric westerly regions as a "wave attractor region" and the two directions of propagation as "forward-" and "backward-accumulation."

$n = 1, k = 5$ mode for $U = 10, 0$ and -10 m s^{-1} basic wind profiles. Fig. 1b shows the results of a series of computations over a range of k similar to those that produced Fig. 1a contours of the turning latitude of equatorially trapped Rossby waves with $n = 1$ as a function of the basic zonal wind and longitudinal wavenumber. The dashed line A–B shows the change in the turning latitude as a mode moves from the easterlies to the westerlies. Zhang and Webster showed that the variation in turning latitude was caused by the change in the ambient potential vorticity gradient. In the regions of easterlies, the effective β-effect decreases; in the westerlies, the effective β-effect is enhanced. Thus, the local Rossby restoring force, and hence the degree of equatorial trapping, becomes a strong function of the sign of the zonal wind. Therefore, within the confines of a rather simple system, Zhang and Webster suggested that the WC mode emanation could be interpreted as a "swelling" of the equatorially trapped mode as it moves from one environment to another. Such behavior appears to be consistent with the phase locked teleconnection patterns noted observationally by Lau and Phillips (1986) in the 40–60 day period band.

In summary, the locations of energy accumulation regions and emanation of energy of transient modes to higher latitudes appear to be determined *entirely* by the structure of the mean flow at low latitudes, irrespective of the location of the forcing along the equator.

b. *Linearity versus nonlinearity*

Webster and Chang used analytic and linear numerical methods to reach their conclusions regarding the importance of longitudinal variations in the low latitude basic winds. Although the results from the study appeared to be consistent with those of O'Lenic et al. (1985), Samel (1987), Frederiksen and Webster (1988) and Gelaro (1989),[2] all of whom reported on a series of experiments using global spectral models, the numerical model used by WC was linear. This agreement between two very different model types, one a linear free surface barotropic model and the other a fully nonlinear general circulation model, would indicate that the processes occurring in the real tropical atmosphere appear to be ostensibly linear. However, to test this hypothesis and determine how robust the linear results are and how nonlinear interactions may modify the results, we must rerun the experiments conducted by WC with a fully nonlinear model and carefully compare and diagnose the results from the two models.

There have been a number of previous studies that have compared linear and nonlinear results, although most of these were based on either a motionless or a uniform basic state (e.g., Boyd 1980, 1983; Gill and Phillips 1986; Hendon 1986; Van Tuyl 1986, 1987; Sardeshmukh and Hoskins 1988, among others). Only a few studies (e.g., Simmons 1982; Simmons et al. 1983; Branstator 1985) compared linear and nonlinear results within nonuniform climatological mean states. However, we are unaware of diagnostic studies that attempt to illustrate how nonlinear interactions modify linear results.

In the current study we will compare linear and nonlinear results of the WC free surface barotropic model and use them to isolate the important mechanisms that determine tropical wave longitudinal trapping and emanation, and, specifically how the nonlinear interactions modify the linear results, if at all. A principal aim of the study is to determine why the tropical atmosphere appears to retain many aspects of the linear system.

c. *Forcing fields*

In a nonlinear regime, the magnitude of the forcing function becomes very important. In the original Webster and Chang study, the main emphasis was on the location, scale, and duration of the convective forcing function, and because it was a linear study, the magnitude of the forcing was essentially arbitrary. In section 2, we go to some effort to determine an appropriate magnitude for the impulsive transient forcing that appears to possess maximum amplitude in the western Pacific and eastern Indian ocean regions. Clearly, we will have to differentiate between long-term average forcing and the higher frequency aggregates of this forcing.

In section 3, a diagnostic scheme is developed to facilitate the comparison of linear and nonlinear results. The emphasis is on deriving a set of equations that spell out the physical mechanisms of the difference between the linear and nonlinear effects. In the fourth section, the nonlinear results and their dependency on the equivalent depth of the fluid are discussed. Section 5 shows how the nonlinear response evolves over a period of time and in section 6,the physical mechanisms responsible for the linear and nonlinear fields are studied in detail. The discussion is drawn together in the last section.

2. Magnitude, scale and duration of episodic convective heating in the tropical regions: the case for strong episodic forcing

Outgoing longwave radiation (OLR) has been used as a surrogate for precipitation for a number of years (e.g., Arkin and Meisner 1987). Figures 2a and 2b show the boreal summer (upper right-hand panel) and winter (upper left-hand panel) OLR distributions in the equatorial strip. Concentrating on values of OLR < 240

[2] Gelaro studied the influence of perturbations in the tropical western Pacific Ocean on the middle latitudes using the NEPRF general circulation model.

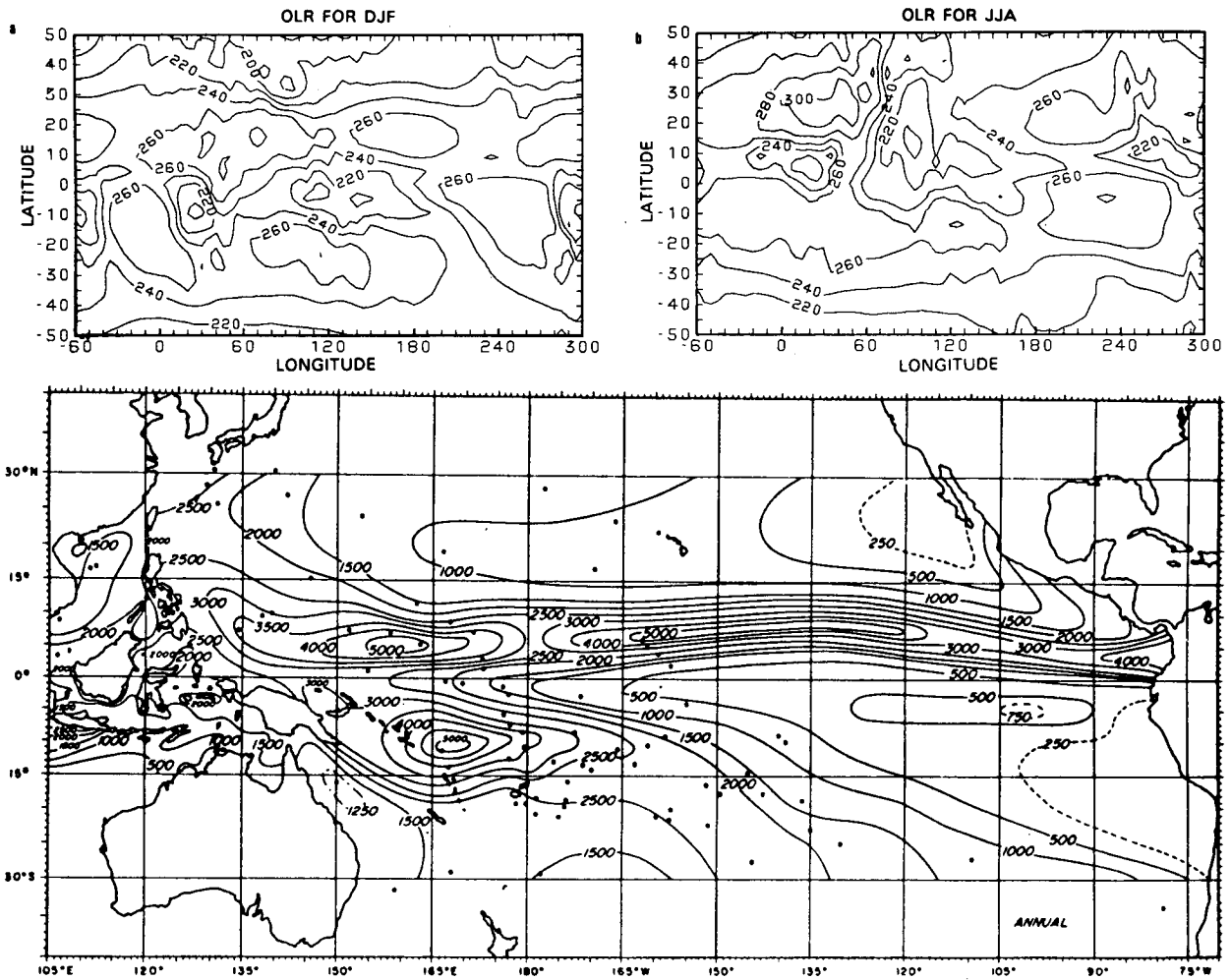

FIG. 2. (a) The boreal winter (DJF), (b) summer (JJA) satellite sensed out-going longwave radiation (OLR; units: W m^{-2}) plotted as a function of longitude and latitude. Fields are averaged using data from 1974–85. (c) The mean annual precipitation estimated from island measurements by Taylor (1973). (units: mm.) Note the similarity of the annual OLR distribution over the Pacific region (Figs. 2a, b) to the rainfall distribution where the 250 W m^{-2} corresponds roughly with the 1500 mm rainfall contour.

W m^{-2}, we note that there are three major minima: over equatorial Africa, over the central Americas and, the largest, over the eastern Indian Ocean and western Pacific Ocean that spans Indonesia. All three centers show an annual cycle with a migration towards the summer hemisphere. At all times of the year, a large minimum remains in the western Pacific Ocean. By extension (Arkin and Meisner 1987), we can infer that intensive precipitation occurs throughout the year. Heating functions derived from such precipitation distributions have been used to drive steady state circulation models in an attempt to model the mean tropical circulation (e.g., Webster 1972,[3] 1981, 1982; Opsteegh and van den Dool 1980; Hoskins and Karoly 1981). To a large degree, these models were able to simulate and explain the strong three-dimensional character of the mean tropical flow.

Accurately assessing the magnitude of the western Pacific Ocean precipitation is rather difficult. Figure 2c presents an estimate of the Pacific Ocean annual precipitation using island data (Taylor 1973). The analysis shows a broad region of precipitation in the western Pacific Ocean of order of 3–5 m and an elongated maximum north of the equator. The first feature appears to be associated with the warm pool region of the western Pacific Ocean (i.e., sea surface temperature >28°C) and the second with the Intertropical Convergence Zone (ITCZ). Whereas it is very difficult to determine absolutely if the magnitudes of Taylor's analysis are representative away from the islands, the satellite estimates of Motell and Weare (1987) indicate that the patterns of precipitation are reasonable, at least. The task is to determine the heating associated with this precipitation, the transient components of the

[3] Actually, in Webster (1972), brightness data was used to infer convective cloudiness and, thence, precipitation and latent heating. Visible brightness data alone, however, provides an ambiguous estimate of precipitation as both stratus layers and desert areas are also bright. Thus, a certain degree of subjectiveness was required.

mean heating and the scale of the divergence associated with them. Measures of the associated divergence are necessary as these are used to drive the free surface barotropic model.

a. Mean heating rates in the warm pool regions

Using an estimate of 3–4 m as the annual precipitation over the western Pacific Ocean from Fig. 2, the equivalent heating rate per unit mass of air can be calculated to be about 2°C day^{-1}. An estimate of the average divergence associated with the heating can be calculated by assuming a rough balance between diabatic heating and the ensuing adiabatic ascent (e.g., Webster 1983). For a simple vertical structure extending through the entire tropical troposphere with a maximum in the middle troposphere, the resulting low level convergence associated with the 2°C day^{-1} heating is 0.6×10^{6} s^{-1}.

We can check this estimate with divergences obtained from the European Centre for Medium Range Weather Forecasting/World Meteorological Organization (ECMWF/WMO) global analysis datasets. The datasets consist of six physical variables at seven standard pressure levels listed twice per day (12 and 00Z) on a 2.5° × 2.5° latitude–longitude grid. Figures 3a and 3b show the annual average (upper panel) and a series of bimonthly averages (lower panels) of the horizontal divergence at 850 mb and 200 mb, respectively, along the equator between 90°E and 150°W for the year 1980.

At 850 mb (Fig. 3a), the region between 140°E and 180°E shows persistent convergence of magnitudes of -1 to -2×10^{-6} s^{-1}. The region of convergence spans the maritime continent of Indonesia extending from the warm waters of the eastern Indian Ocean to the western Pacific Ocean warm pool. During the boreal summer, substantial convergence exists in the Indian Ocean. Very strong upper level divergence is apparent over the Indonesian west Pacific region at all times of the year. Clearly, between Figs. 3a and 3b, it is obvious that there is strong heating in the mean between about 140°E and 180°E. However, Fig. 3 does not show the spatial and temporal scales of the higher frequency organized divergence that aggregates to provide the mean divergence fields.

b. Low frequency variations in the heating rates in the warm pool regions

Figures 4a–d show longitude time sections along the equator of daily values of the divergence (units 10^{-6} s^{-1}) between 90°E and 150°W. Each panel shows two-month segments. Regions of convergence are shaded. By comparing these sections with Fig. 3, we can see that the moderate values of net convergence are replaced with large amplitude, low frequency features. Indeed, values often exceed -5×10^{-6} s^{-1} for periods of days and on scales of order 3000–5000 km. That is, the annual divergence pattern over the warm pool regions is made up of a series of strong episodic events. Such events have been referred to as "super clusters" by Nakazawa (1988) and Lau et al. (1989). Figure 4 indicates that the "super clusters" are associated with convergence with magnitudes of an order of magnitude greater than the annual mean. Thus, the heating rates associated with the episodic events range from 10° to 20°C day^{-1} and have typical periods of days and longitude scales of 3000–5000 km.

c. Formulation of a realistic transient tropical heating function

We utilize a free surface barotropic model (see Webster and Chang 1988 and section 3 of this paper). In such a system, an equivalent divergence function acts as a mass source–sink function. With the divergence fields displayed in Fig. 4 in mind, we define an appropriate transient forcing function as

$$m(x, y, t) = EJ(x, y)\tau(t) \tag{3}$$

where E is the mass source–sink amplitude and J and τ are the spatial and temporal functions. The magnitude of E depends on the equivalent depth. For a 2000 m equivalent depth, the value of E is set at 5×10^{-3} m s^{-1}:

$$J(x, y) = \exp\left(-\frac{|x - x_0|}{2}\right)\exp\left(-\frac{|y - y_0|^2}{4}\right) \tag{4}$$

and

$$\tau(t) = (t^3/2\Delta^3)\exp(-t/\Delta) \tag{5}$$

where Δ is set at 2 days.

Figure 5a shows the variation of the amplitude function with respect to time [i.e., $\tau(t)$]. The left-hand ordinate scale shows the mass source term while the right-hand scale shows the equivalent divergence associated with the episodic forcing. The equivalent divergence is calculated from (3) and the linear model of WC. The lower curve in Fig. 5a shows the amplitude function used in WC linear calculations. Figure 5b plots the assumed horizontal distribution function $J(x, y)$ in the western Pacific region.

3. Decomposition of the steady state, linear and difference fields

The model used in the study is identical to that used by Webster and Holton (1982) and Webster and Chang (1988). The model is a free surface barotropic equatorial channel model with boundaries at 60°N and 60°S. The numerical schemes are semi-implicit in time and semispectral in space. The governing equations are

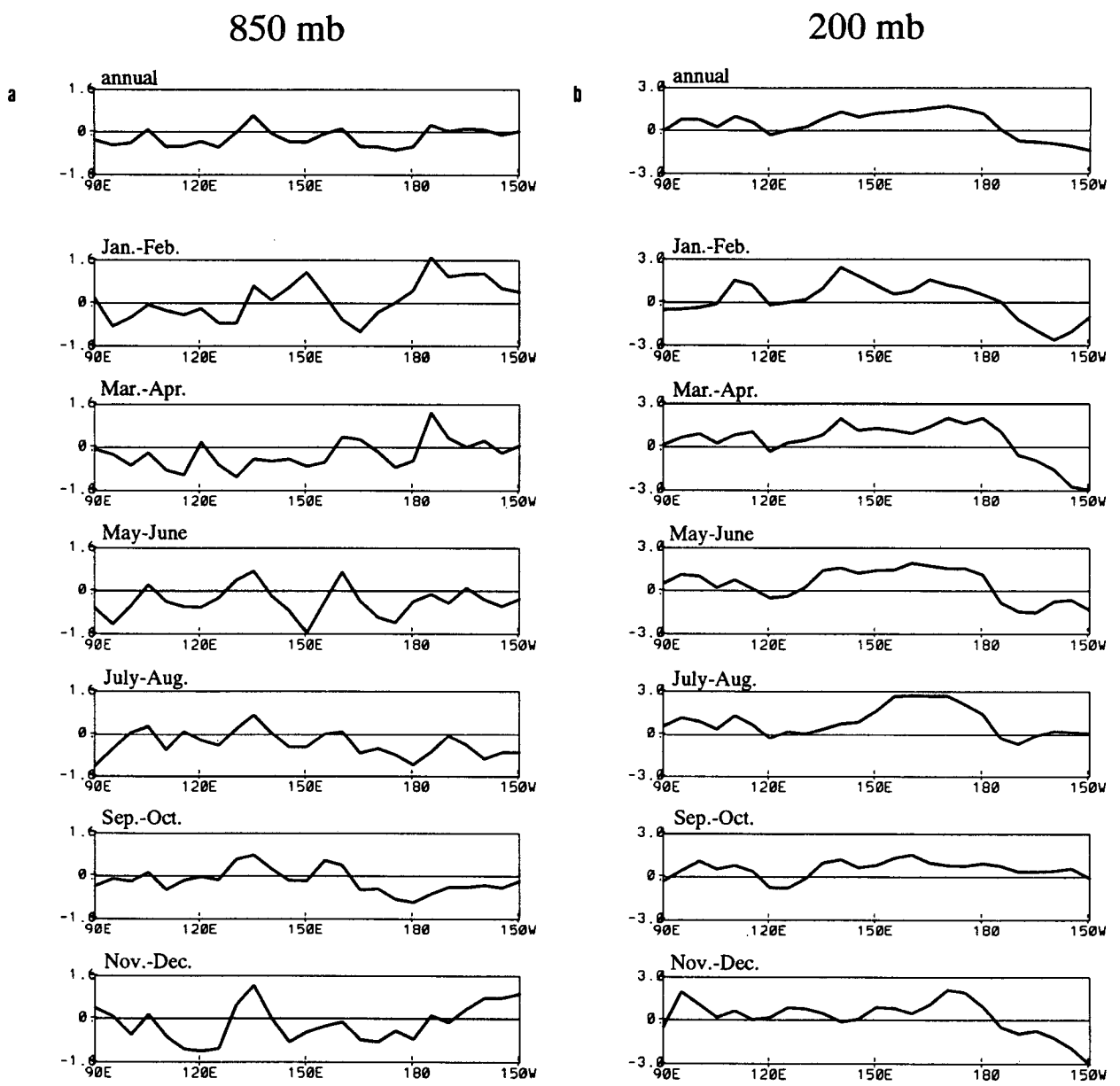

FIG. 3. Longitude sections of the 850 mb (left column) and the 200 mb (right column) divergence plotted around the equator for the year 1980. Top diagram shows the annual divergence distribution. The lower panels show the mean two-monthly values. Units: 10^{-6} s^{-1}.

$$\frac{\partial U}{\partial t} - fV + I(U) = -g\frac{\partial H}{\partial x} - \alpha(U - \delta_0 U_b) \quad (6)$$

$$\frac{\partial V}{\partial t} + fU + I(V) = -g\frac{\partial H}{\partial y} - \alpha V, \quad (7)$$

and

$$\frac{\partial H}{\partial t} + I(H) = M, \quad (8)$$

in which U and V represent longitudinal and latitudinal velocity components, H represents the depth of the fluid, M is the mass source or sink distribution that forces the system, α the coefficient of the Rayleigh damping, U_b a zonally symmetric climate state, and δ_0 a Dirac delta function that is zero for all components of the basic state except for the zonally symmetric state U_b. Here $I(U)$, $I(V)$, and $I(H)$ are the nonlinear terms:

$$I(U) = U\frac{\partial U}{\partial x} + V\frac{\partial U}{\partial y} \quad (9)$$

$$I(V) = U\frac{\partial V}{\partial x} + V\frac{\partial V}{\partial y} \quad (10)$$

and

$$I(H) = \frac{\partial}{\partial x}(UH) + \frac{\partial}{\partial y}(VH). \qquad (11)$$

The map scale factors have been omitted from (6)–(11) for simplicity. However, they are included in Webster and Holton's (1982) formulation.

To produce an initial mean steady state with a longitudinal and latitudinal structure, system (6)–(8) is integrated with a steady forcing [i.e., a time invariant form of M in (3)] in the same manner as in WC until a steady state response is reached. The functional form of M in (8) is identical to (46) of Webster and Chang (1988). Figure 6 shows the mean wind and height field

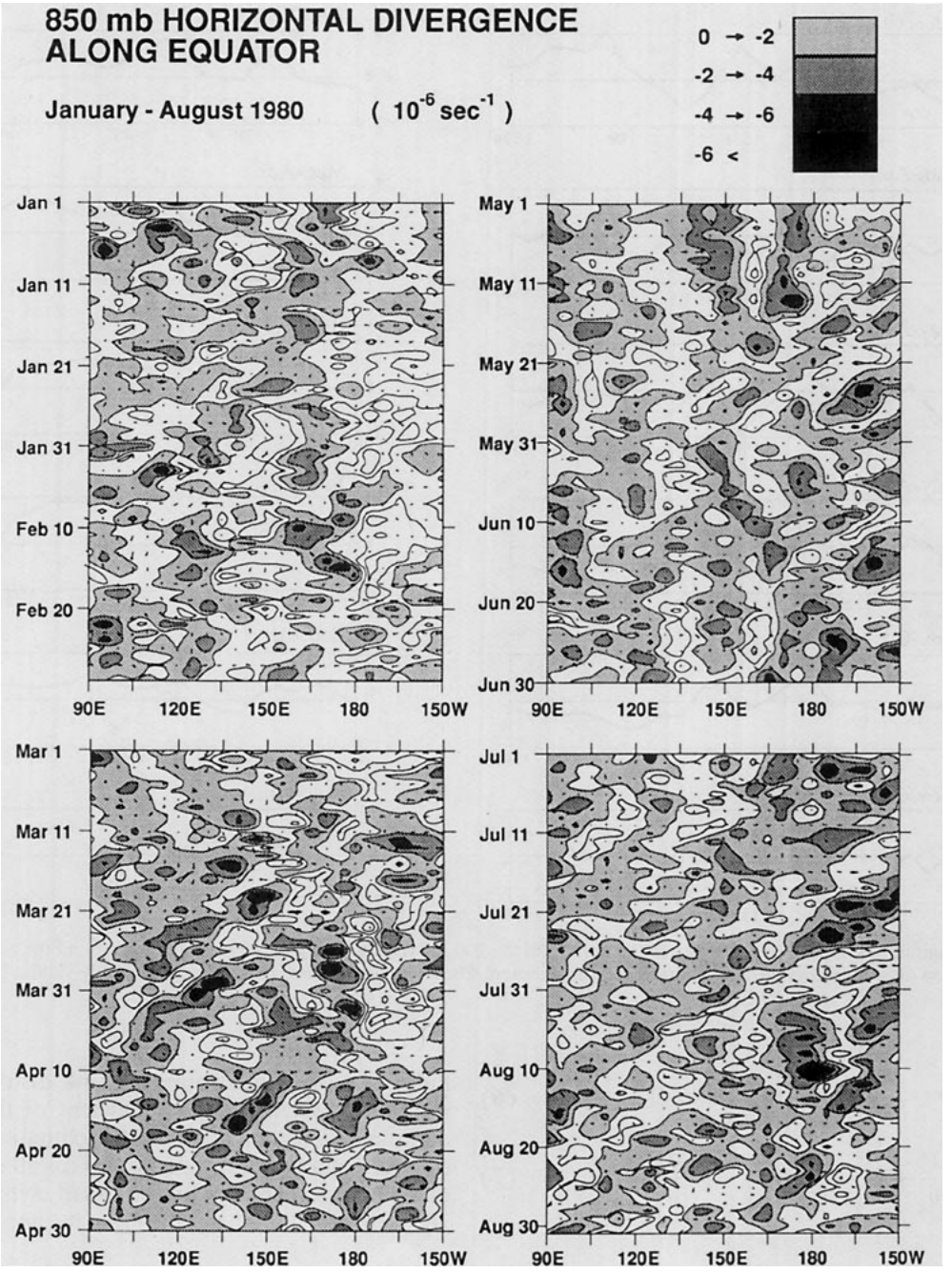

FIG. 4. Time-longitude sections of the 850 mb divergence fields plotted between 90°E and 150°W. The sections show the substructure of the first four mean bimonthly lower tropospheric divergence fields shown in the left column of Fig. 3. Shaded areas denote convergence. Heavier shading indicates convergence >2 $\times 10^{-6}$ s^{-1} and the heaviest shading >4 $\times 10^{-6}$ s^{-1}. Note the prolonged periods of convergence occurring along broad regions along the equator.

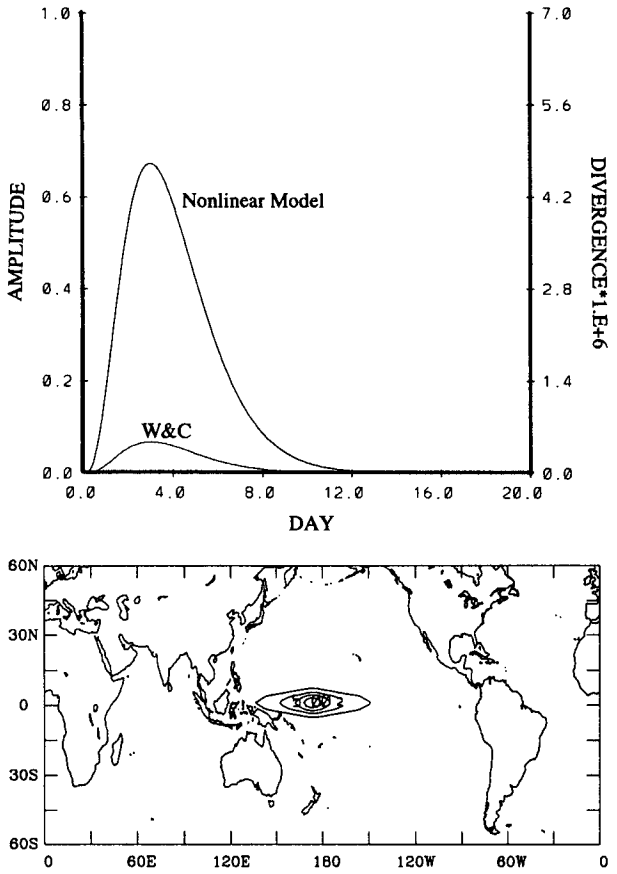

FIG. 5. (a) The time evolution of the forcing function defined in (1). The right-hand side refers to the equivalent divergence (units: 10^{-6} s^{-1}). (b) The spatial distribution of the forcing is normalized to a value of 5.

distributions so produced, which correspond to the "strong westerly" case of WC (their Fig. 12a). The points A, B, C and D in Fig. 6 are the centers of the transient forcing used in WC.

In order to illustrate the nonlinear effect more clearly, we rearrange the governing equations in the following manner. First, we separate the total responses as

$$U(x, y, t) = U_s(x, y) + u_n(x, y, t)$$
$$V(x, y, t) = V_s(x, y) + u_n(x, y, t)$$
$$H(x, y, t) = H_s(x, y) + h_n(x, y, t)$$
$$M(x, y, t) = M_s(x, y) + m_n(x, y, t) \quad (12)$$

where the subscripts s and n indicate the steady state basic flow and the nonlinear response.

In order to differentiate between the linear and nonlinear responses, we define the following difference fields as

$$u_d = u_n - u_l$$
$$v_d = v_n - v_l$$
$$h_d = h_n - h_l \quad (13)$$

where the subscripts l and d denote the linear fields and the difference between the nonlinear and linear fields, respectively.[4]

Substituting (12) and (13) into (6)–(11) allows the equations to be broken into four sets representing the steady background fields and the nonlinear, linear, and difference fields, respectively. The background fields must be governed by the following set:

$$U_s \frac{\partial U_s}{\partial x} + V_s \frac{\partial U_s}{\partial y} - fV_s + g \frac{\partial H_s}{\partial x} + \alpha(U_s - \delta_0 U_b) = 0 \quad (14)$$

[4] The linear set of equations has the same form as that in WC and are not repeated here for brevity. Interested readers can refer to section 4 of WC.

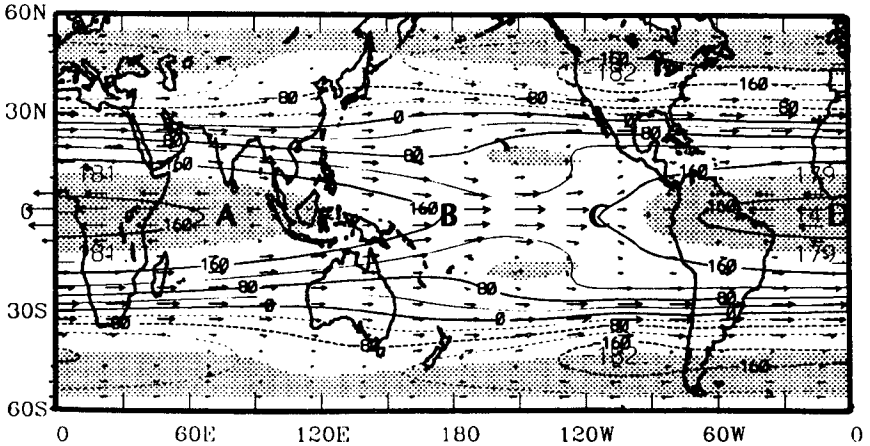

FIG. 6. The basic fields used in the study. Vector arrows denote the wind field. The longest vector is 30 m s^{-1}. The contours represent the height field (units: m). The shaded areas show the location of the easterly winds, B shows the location of the forcing shown in Fig. 5.

$$U_s \frac{\partial V_s}{\partial x} + V_s \frac{\partial V_s}{\partial y} + fU_s + g \frac{\partial H_s}{\partial y} + \alpha V_s = 0 \quad (15)$$

and

$$\frac{\partial}{\partial x}[(H_{00} + H_s)U_s] + \frac{\partial}{\partial y}[(H_{00} + H_s)V_s] = M_s, \quad (16)$$

in which H_{00} represents the domain-averaged depth of the fluid. Equations (14)–(16) are solved numerically as described by WC. For a given M_s, the set is integrated in time until a steady state solution is obtained. Figure 6 shows the basic field used in the study, which was produced by integrating the sets of (14) to (16) until convergence occurred. The shaded areas denote the easterly regimes. The letters signify the locations of forcing used in the WC study.

The linear, nonlinear, and difference field governing equations may be obtained by setting $i = l$, n, and d, respectively in the following set:

$$\frac{\partial u_i}{\partial t} + X_i + Lu_i - fv_i + g \frac{\partial h_i}{\partial x} = 0 \quad (17)$$

$$\frac{\partial v_i}{\partial t} + Y_i + Lv_i + fu_i + g \frac{\partial h_i}{\partial y} = 0 \quad (18)$$

and

$$\frac{\partial h_i}{\partial t} + Z_i + Lh_i = m_i(x, y, t) \quad (19)$$

where $m_i(x, y, t) = 0$ if $i = d$, and the operators are defined as

$$Lu_i(x, y) = \frac{\partial}{\partial x}(U_s u_i) + \frac{\partial}{\partial y}(V_s u_i) \quad (20)$$

$$Lv_i(x, y) = \frac{\partial}{\partial x}(U_s v_i) + \frac{\partial}{\partial y}(V_s v_i) \quad (21)$$

and

$$Lh_i = \underbrace{H_{00}\left(\frac{\partial u_i}{\partial x} + \frac{\partial v_i}{\partial y}\right)}_{\text{A}} + \underbrace{\frac{\partial}{\partial x}(H_s u_i) + \frac{\partial}{\partial y}(H_s v_i)}_{\text{B}} \quad (22)$$

Here X_i, Y_i and Z_i are the nonlinear operators that are zero for $i = l$. They are defined as

$$X_i = u_n \frac{\partial u_n}{\partial x} + v_n \frac{\partial u_n}{\partial y} \quad (23)$$

$$Y_i = u_n \frac{\partial v_n}{\partial x} + v_n \frac{\partial v_n}{\partial y} \quad (24)$$

and

$$Z_i = \frac{\partial}{\partial x}(h_n u_n) + \frac{\partial}{\partial y}(h_n v_n). \quad (25)$$

In the following sections, we will force the nonlinear and linear models with the episodic forcing described in section 2. These two systems will be analyzed and the robustness of the WC accumulation–emanation theory, that is, the degree to which the theory transcends nonlinearity, will be tested.

4. Nonlinearity and equivalent depth dependencies

Figure 7 shows longitude time sections along the equator of the zonal velocity perturbation for two different equivalent depths, 2000 m and 500 m. The 2000 m depth is the same as that chosen by WC. In each case, the linear, nonlinear, and difference fields, as given by (17)–(25), are shown. The motion was forced by the function displayed in Fig. 5 and functions (4) and (5) at location B in Fig. 6.

There are two principal features evident in Fig. 7. The first is that there is a great similarity between the responses of the two fluids of different equivalent depths. Both show accumulation in the region of negative stretching deformation (cf., Fig. 6), which occurs at roughly the same time. One of the major differences, however, is that to the west of the accumulation zone, the power of the very long waves is greater in the deeper fluid in both the linear and nonlinear cases. The reason for the difference is quite simple. Webster and Chang show that the westward group and phase velocities increase with increasing equivalent depth, especially for the longest longitudinal mode. They also show that if the initial group speed of the mode is sufficiently strong and westward, the mode could pass through the accumulation zone and continue its equatorial migration. Clearly, the long waves apparent in the 2000 m fluid are the longest, most rapidly propagating modes, much more rapid, in fact, than their equivalent modes in the shallower fluid. The second feature of note is that the differences that do occur between the linear and nonlinear responses happen in the regions of maximum negative stretching deformation; i.e., in the accumulation region itself as shown in the difference fields in the bottom panels. The upper panels of Fig. 7 also indicate that the larger-scale nonlinear waves appear to penetrate through the accumulation zone with less difficulty than the similar scale linear waves. We will examine these differences in section 6. Another feature of Fig. 7 is that there are indications that the wave propagation is not completely westward; propagations also move eastward toward the accumulation zone. The evolution of the nonlinear response is discussed in the following section.

5. Evolution of the nonlinear response

As geopotential perturbations are inherently small at low latitudes (see e.g., Webster 1983), the modal evolution is easier to follow using the divergence field. Figure 8a shows a series of latitude–longitude sections of the divergence during the first 19 days of integration

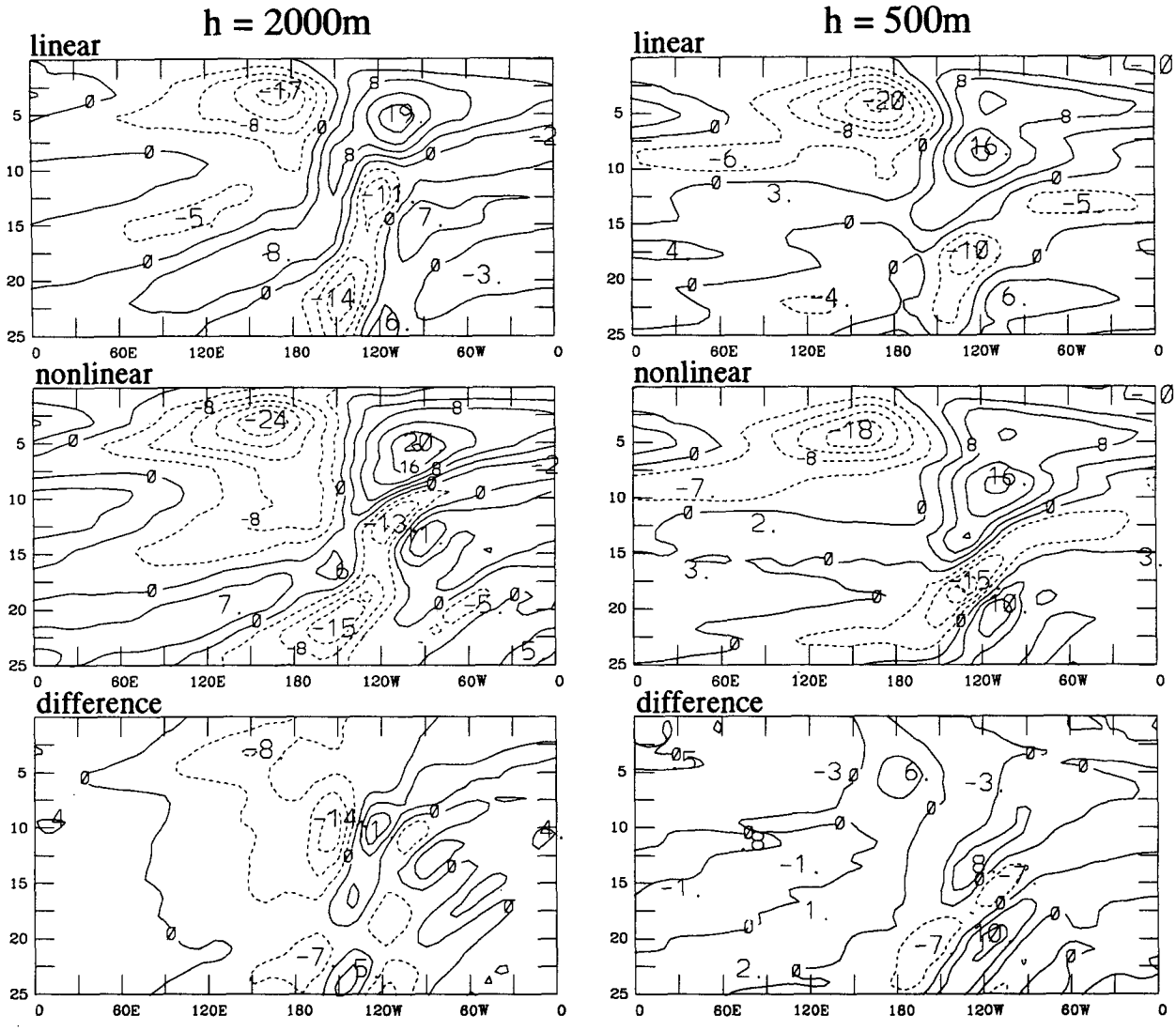

FIG. 7. Time-longitude plots of the zonal velocity component (units m s^{-1}) around the equator of the linear (upper panels), nonlinear (middle) and the difference fields (bottom) for fluids of equivalent depths of 2000 m (left column) and 500 m (right column).

using the same parameters as were used in the calculations shown in Fig. 7 for a 500 m equivalent depth field. In all sections, the shaded region indicates the easterly background winds of Fig. 6. Following the imposed episodic forcing in the central western Pacific, a rather complicated mode structure appears along the equator moving both eastward and westward away from the source. Given the symmetry of the forcing about the equator, the responses are also symmetric. Later in the integration, considerable influences occur at higher latitudes. Comparing the results with those shown by WC, emanation from the accumulation region is apparently a common feature of both the linear and nonlinear regimes and in both deep (not shown) and shallow fluids.

Figure 8b provides a summary of the characteristics of the wave packets along the equator as a function of time. The paths of different wave packets are identified from a time and longitude cross section of divergence field along the equator.[5] The characteristics of the three Rossby wave packets as functions of time and longitude (labeled as Rossby *1*, *2*, and *3*) and the Kelvin wave (*K*) are shown. Such extensions occur only for a Rossby wave in the vicinity of the equatorial westerlies. The detailed evolution of the response away from the source region may be described as follows. The heavy double line shows the characteristic of the nondispersive Kelvin mode. In a 500 m equivalent depth fluid, the mode

[5] The character of the divergence field can be found in the top panel of Fig. 11, which shows the evolution of term *A* of (22) or H_{00} $[(\partial u_i/\partial x) + (\partial v_i/\partial y)]$.

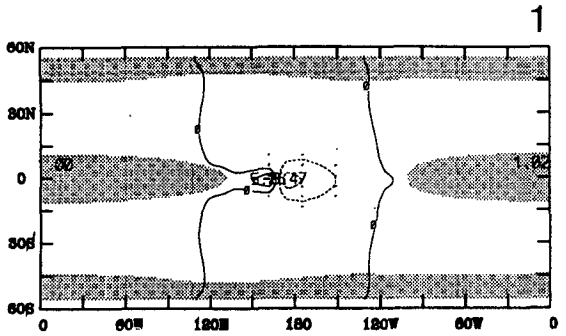
1
60N
30N
0
30S
60S
0
60E
120E
180
120W
60W
0
.00
-.37
1.02

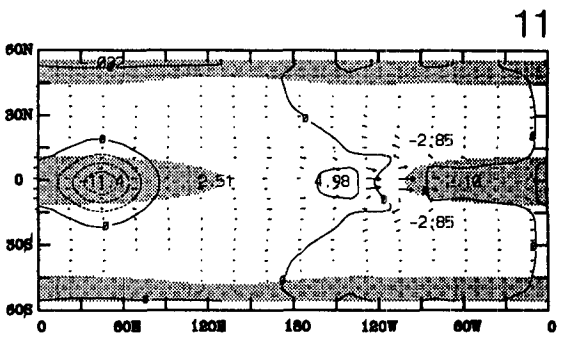
11
60N
30N
0
30S
60S
0
60E
120E
180
120W
60W
0
.02
-2.85
-11.4
2.51
.98
-1.10
-2.85

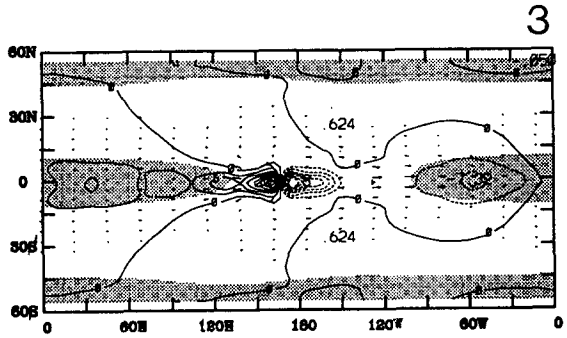
3
60N
30N
0
30S
60S
0
60E
120E
180
120W
60W
0
.624
.624

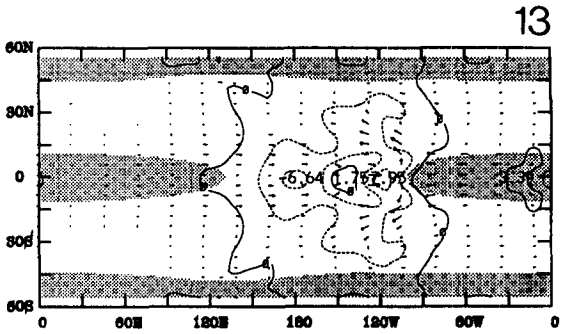
13
60N
30N
0
30S
60S
0
60E
120E
180
120W
60W
0
-6.64
1.51
.98

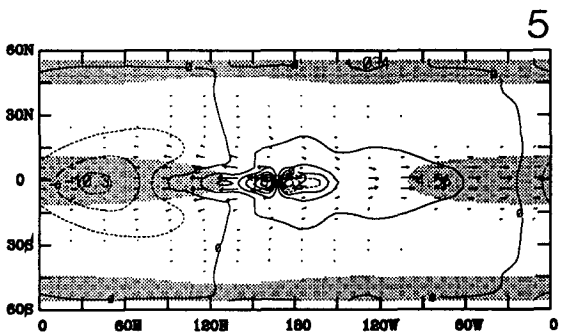
5
60N
30N
0
30S
60S
0
60E
120E
180
120W
60W
0
-10.3

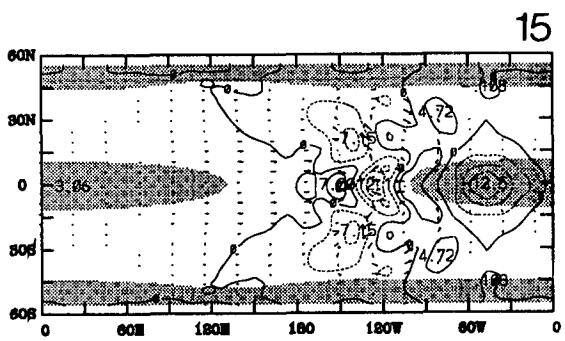
15
60N
30N
0
30S
60S
0
60E
120E
180
120W
60W
0
4.72
-7.15
-1.06
-7.15
4.72

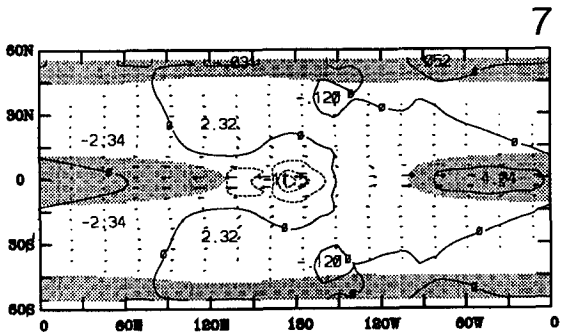
7
60N
30N
0
30S
60S
0
60E
120E
180
120W
60W
0
2.32
-2.34
-2.34
2.32

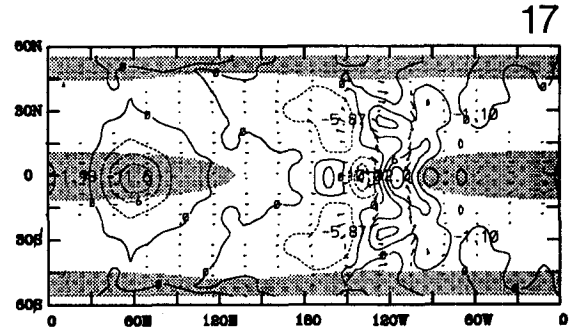
17
60N
30N
0
30S
60S
0
60E
120E
180
120W
60W
0
-5.87
-5.87

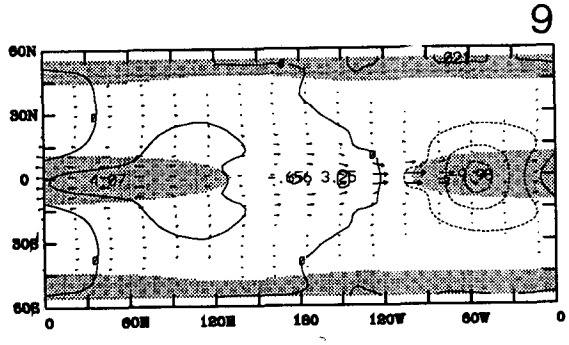
9
60N
30N
0
30S
60S
0
60E
120E
180
120W
60W
0
1.07
.656
3.85

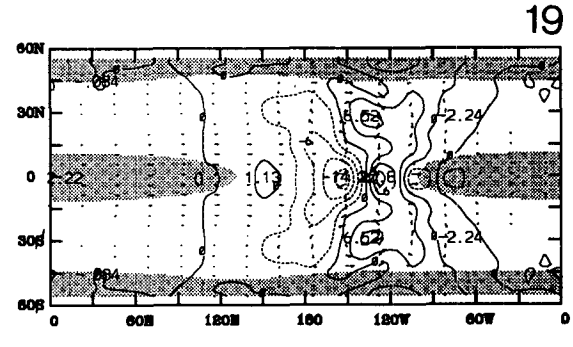
19
60N
30N
0
30S
60S
0
60E
120E
180
120W
60W
0
-2.24
-2.24

propagates at 70 m s^{-1} or 60° of longitude per day. Two slowly moving packets (Rossby *1* and *2*) move eastward and westward away from the source region. These diverging characteristics represent the effect of the two-way accumulation of Rossby waves described in section 1 (Webster et al. 1989). The shorter eastward propagating packet (Rossby *1*) reaches the accumulation zone within a few days. On the other hand, the westward propagating long wave packet (Rossby *2*) takes nearly two weeks to reach the negative stretching deformation regions, at least those defined by the simple flow shown in Fig. 6. A third mode (Rossby *3*) becomes apparent (see Fig. 7) at about day 11. As the modes approach the equatorial westerlies, their longitudinal scale changes substantially as they expand poleward (i.e., swell) as predicted by Zhang and Webster (1989). Thus, irrespective of the sign of the initial propagation along the equator, the mode appears to accumulate into the negative stretching deformation region near the westerly maximum along the equator.

The hatched area in Fig. 8b shows when the mode packets extend substantially toward higher latitudes. Entering the region of equatorial westerlies first, Rossby *1* "swells" first towards higher latitudes. As Rossby *2* and *3* take substantially longer to reach the westerlies, they do not influence higher latitudes until much later.[6] Figure 8c shows time sections along the two meridians 160°E (upper panel) and 120°W (lower panel) between 60°N and 60°S of the perturbation zonal velocity for the first 25 days of integration. The first section, which passes directly through the forcing, shows a strong local response trapped closely to the equator. After the initial excitation, the region is undisturbed until the return of the successive Kelvin wave packets around days 7, 14 and so on, and by the low frequency long waves that have propagated through the accumulation region. Little variability occurs at higher latitudes along this meridian until day 20. The second section passes directly through the accumulation zone

[6] In the context of our model we refer to the higher latitudes beyond the limit of the equatorial easterlies, as indicated in Figure 6a.

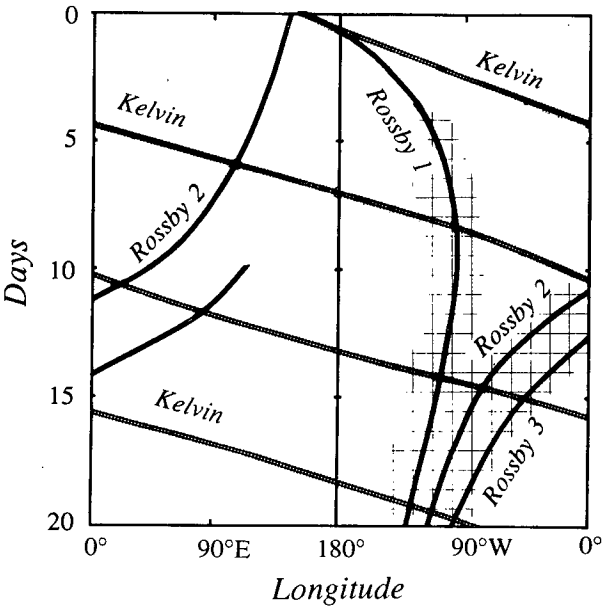

FIG. 8b. The characteristics of the Rossby *1*, Rossby *2* and Rossby *3* modes and the Kelvin mode (*K*) obtained from Fig. 8a. The hatching refers to the time when the mode extends substantially into the extratropics. Note that the extension does not commence until the mode packet, either through eastward or westward propagation, enters the region of the equatorial westerlies.

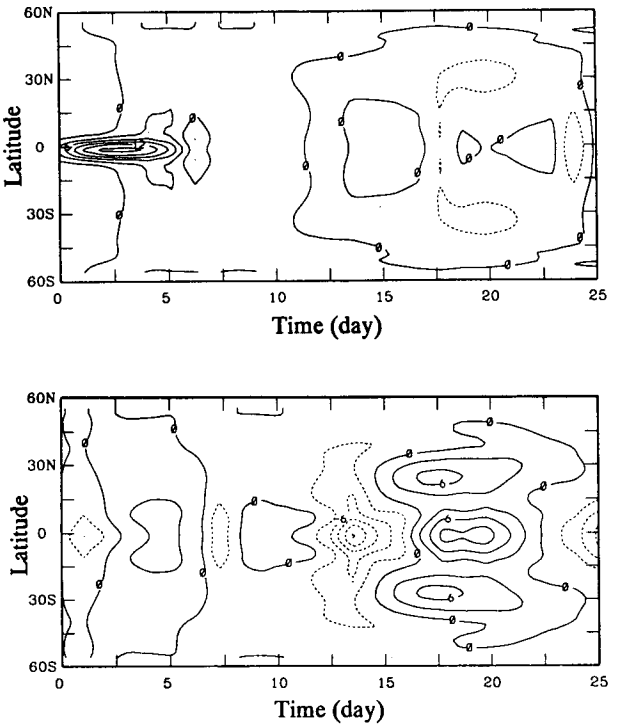

FIG. 8c. Latitude time sections along meridians 160°E (upper panel, section through the forcing region) and 120°W (lower panel, section through the equatorial westerlies) of the divergence field (units: 10^{-6} s^{-1}).

FIG. 8a. Time evolution of the nonlinear divergence field (units: 10^{-7} s^{-1}) for a fluid with h = 500 m forced at location *B* in Fig. 6. Plots are shown at two day intervals for the first 19 days of integration. The sequence shows families of modes moving along the equator and emanating towards higher latitudes in the vicinity of the equatorial westerlies. The basic field is identical to that shown in Fig. 6 with the area of easterlies shaded for easier reference. The modal characteristics that make up the sequence are summarized in Fig. 8b. The longest vector represents 20 m s^{-1} and the contour interval is 3×10^{-7} s^{-1}.

defined from Fig. 7. Rather rapid perturbation along the equator occurs that "swells" into the higher latitudes after approximately a week to twelve days. This earlier extension into the higher latitudes is a manifestation of the eastward propagation of the slow Rossby wave packet [i.e., the forward accumulation process of Webster et al. (1989)] discussed above. The important aspect to be noted here, though, is that the perturbation of the higher latitudes in the vicinity of the equatorial westerlies occurs well in advance of the perturbation at higher latitudes near the longitudes of forcing. The preferential propagation in the westerlies appears to be consistent with the theoretical works of Hoskins and Karoly (1981), Lim and Chang (1983), Zhang and Webster (1989) and many others. Although the first two works focus on stationary waves, and all considered simpler zonally averaged states than considered here, all studies found greater lateral propagations in westerly rather than in easterly basic states.

6. Diagnostics of the nonlinear fields

Figure 7 indicated that there was considerable similarity between the linear and nonlinear results. The difference fields, however, though small over most of the domain were largest in the accumulation zone. Despite these differences, the phenomena of accumulation appeared to extend from the linear to the nonlinear regime. In order to understand the modifications made by the nonlinearity of the system, and to understand why the impact is relatively minor, it is necessary to consider the individual components of the set (17)–(19).

Figures 9 and 10 show longitude time sections of the components of the zonal wind equation (17) averaged over the bands 0° to 10°N and 30°N to 40°N, respectively. The fields shown are the linear advection terms (Lu_n, defined in 20), the Coriolis term (fv_n), the zonal pressure gradient ($g\partial h_n/\partial x$), the nonlinear advection (X_i) and the ageostrophic zonal wind component ($-fv_n + g\partial h_n/\partial x$). To decipher the important physical processes, it is necessary to separate the equatorial strip into two regions, the accumulation region near 120°W and the remainder of the domain. Away from the accumulation zone, the flow is basically geostrophic with the Coriolis term being balanced by the zonal pressure gradient. Here, the ageostrophic term only assumes considerable values periodically with the passage of the Kelvin wave. Within the accumulation zone, the balances become much more complicated. The ageostrophic and nonlinear terms increase by over two orders of magnitude. At higher latitudes (Fig. 11), the flow is effectively geostrophic until about day 10, at which time the ageostrophic and nonlinear terms grow considerably. Note, though, that these terms grow in the longitudes of the accumulation zone, which we have anticipated from Fig. 8c. Clearly, the nonlinearities and ageostrophic motions are a result of processes originating in the accumulation zones of the equatorial westerlies.

Figures 11 and 12 show the components of the h-equation (19) averaged between 0°–10°N and 30°N–40°N in the same time-longitude form as in Figs. 9 and 10. The panels show, respectively, the divergence term (A in 22), the h-advection term (B in 22) and the nonlinear terms (Z_i in 25). Basically, the structure is very similar to the momentum equations. The terms are generally bigger in the accumulation zone than elsewhere except with the passage of the Kelvin wave that is highly divergent. The passage may be seen in the large values of divergence propagating eastward. The nonlinear terms do not become large at higher latitudes until a number of days have passed.

Early in the integration, the divergence term, reflecting the forcing function, is dominant. Later in the integration, the structure of the terms in the continuity equation is very similar to the momentum equation. The initial large amplitude of the divergence makes it difficult to compare the relative significance of the different terms in (19). However, if we set $i = d$ in (22), the difference fields simplify the comparison simply because the initial divergence fields have very similar magnitudes in the linear and nonlinear domains. Figures 13 and 14 repeat the diagnostics of the height equation shown in Figs. 11 and 12, except for the difference fields. From the last panels of Figs. 13 and 14, it is clear that the nonlinear interactions between the velocity and mass fields are important in creating the differences between the linear and nonlinear results at low latitudes, but of little consequence at higher latitudes. We have also calculated the difference terms within the zonal momentum equation [i.e., by setting $i = d$ in (17)]. Here the effects of the nonlinear interactions [i.e., X_i in (17)] are not so obvious when compared to Fig. 13. Thus, the model results suggest that the differences between linear and nonlinear fields first appear in the mass fields. Subsequent differences in the momentum fields reflect and nonlinear interactions between the mass and velocity fields.

In summary, there appears to be significant variability in the magnitude of the terms of the equations between the accumulation region and the rest of the domain. However, if we return to the earlier figures (note, especially, Fig. 7), there appears to be very little difference between the linear and nonlinear responses, even when realistic values of forcing were used. That is, accumulation still occurs in the regions of negative stretching deformation even though the differences between the linear and nonlinear fields maximize in this region. Probably, the reason for the similarity is that the ageostrophic and nonlinear advection terms tend to cancel each other. In other words, the difference fields of Fig. 7 are comprised principally of phase dif-

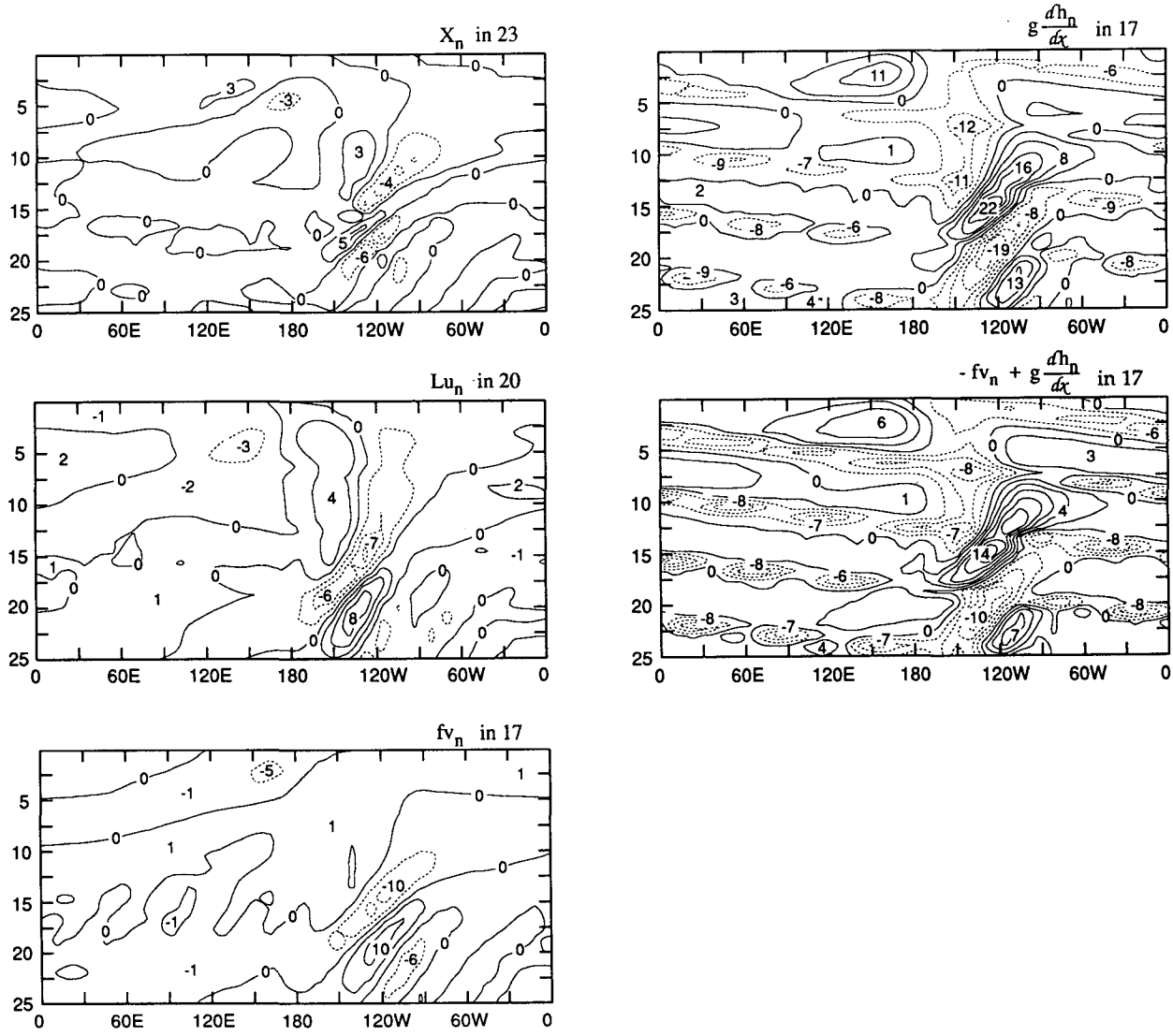

FIG. 9. Diagnostics of the nonlinear zonal momentum equation as a function of time and longitude averaged between the equator and 10°N (units: 10^{-6} s^{-1}). Terms are described in the text.

ferences of linear and nonlinear waves. That is, the wave energy accumulation mechanism is sufficiently robust to transcend linearity and nonlinearity for realistic parameter ranges.

7. Conclusions

a. Linear and nonlinear accumulation and emanation

In this study we have studied the response of the tropical atmosphere to episodic forcing of realistic magnitude to see if the feature of energy accumulation, evident in earlier linear studies (WC, Frederiksen and Webster 1988), was sufficiently robust to exist in the nonlinear regime. It was the intent of the study to determine the dominant mechanisms that produce the differences, if any, between the linear and nonlinear results. To facilitate the study we have systematically diagnosed the linear and nonlinear forced responses in a steady mean state that varies both in longitude and latitude. The basic state, shown in Fig. 6, contains both shearing and stretching deformations with magnitudes and forms found in the atmosphere.

A number of general conclusions regarding the response of the tropical atmosphere to episodic forcing can be drawn. These are

(i) The phenomenon of energy accumulation of transient equatorially trapped modes exists in the non-

linear domain in a fashion very similar to linear response. Regions where the stretching deformation is positive (i.e., $\partial U/\partial x > 0$) are regions of wave action flux (wave energy density) divergence. On the other hand, regions where $\partial U/\partial x < 0$ are regions of wave action flux convergence. Thus, just as in the linear domain, the region of convergence occurs to the east of the maximum westerly wind relative to forcing at any location along the equator. In that sense, the distributions appear to match observations quite well. Figure 15 shows a result from the diagnostic study of Webster and Song (1989). The dashed curve shows the variation of the local perturbation kinetic energy from a zonal average (i.e., PKE*) averaged between 5°N and 5°S. The solid line shows the distribution of U in the same latitude band. Both curves represent longterm average boreal winter mean values. Note the correspondence between the regions of PKE* > 0 and $U_x < 0$.

(ii) The nonlinear experiments show that wave energy accumulation appears to occur in the negative stretching deformation region of the basic flow for both the eastward propagating shortwave packets and the westward propagating longwave packets. The results substantiate, to a large degree, the theoretical results of Webster et al. (1989). The eastward propagating wave packet, due to the proximity of the forcing to the westerlies, reaches the westerlies much earlier than the westward packet, thus influencing the extratropics

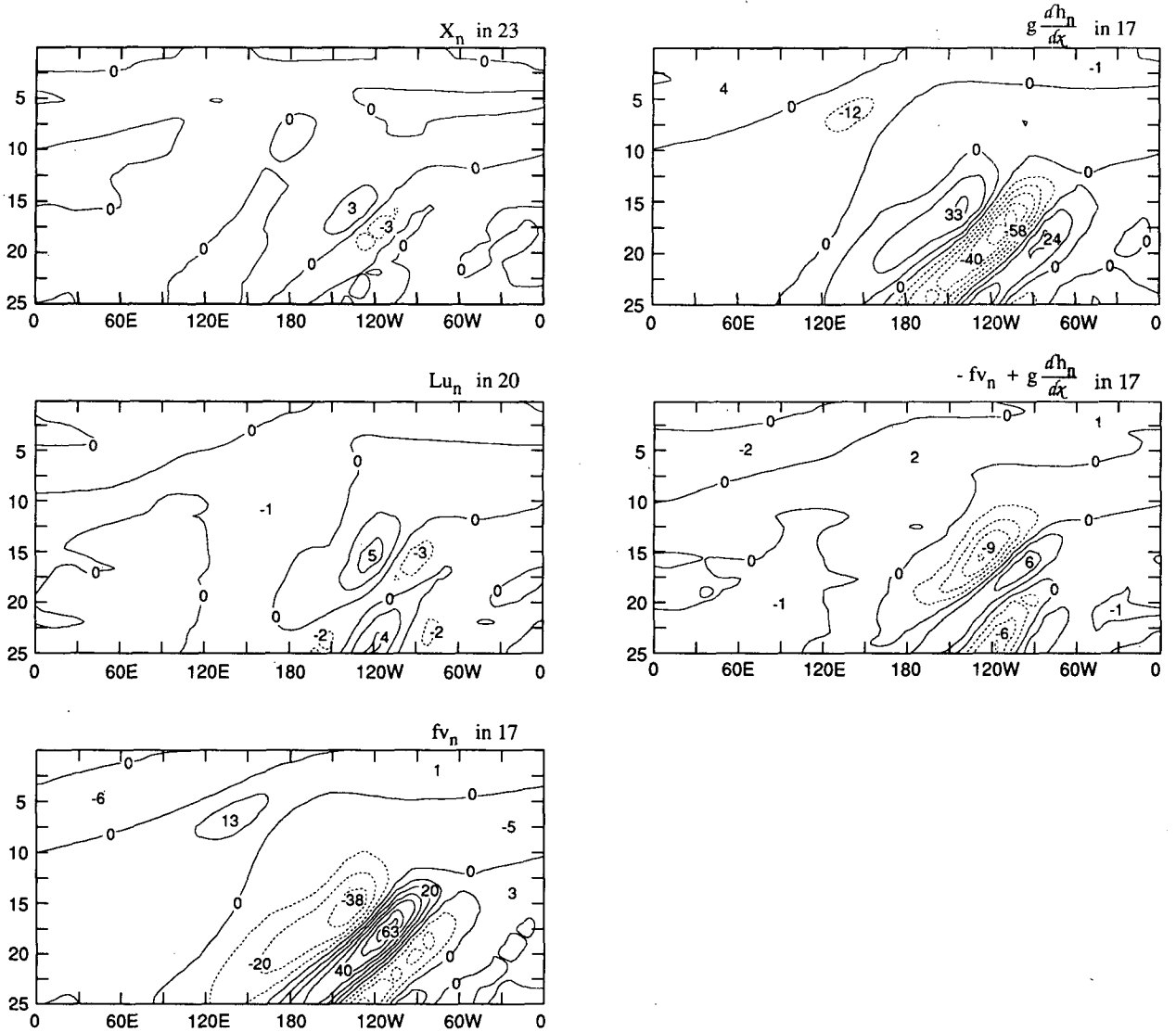

FIG. 10. Diagnostics of the nonlinear zonal momentum equation as a function of time and longitude averaged between 30°N and 40°N (units: 10^{-6} s^{-1}). Terms are described in the text.

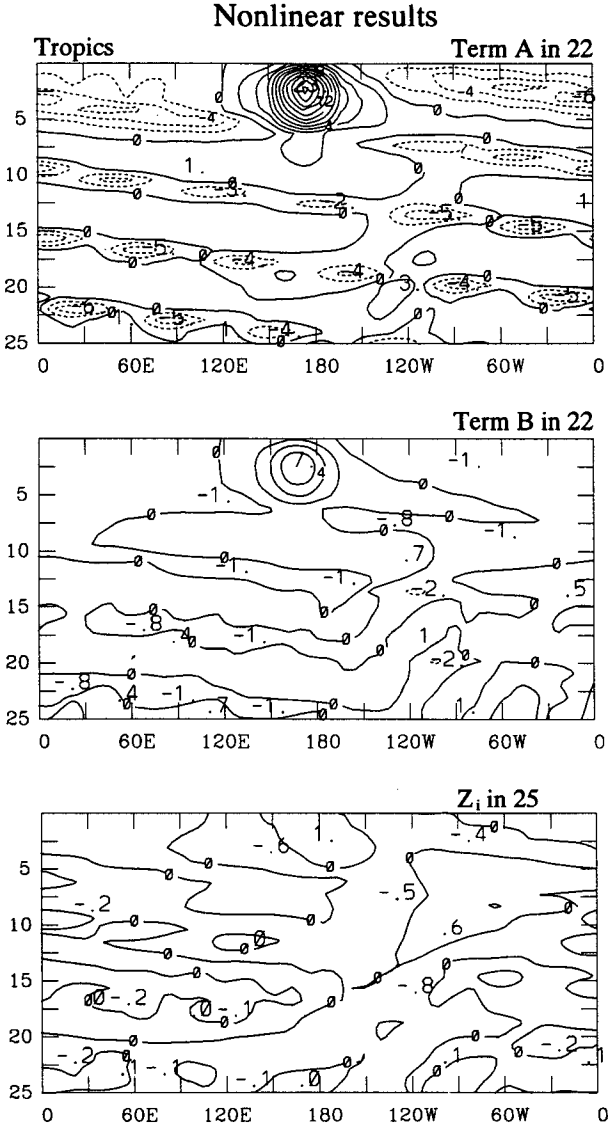

FIG. 11. Diagnostics of the nonlinear height or continuity equation as a function of time and longitude averaged between the equator and 10°N (units: 10^{-5} s^{-1}). Terms are described in the text.

much earlier where extensive lateral "modal swelling" occurs, as predicted by Zhang and Webster (1989).

(iii) Both the linear and nonlinear results show a relative independence to the equivalent depth of the fluid as indicated by the similarity of the response to forcing for 2000 m and 500 m fluids. The only difference is that the accumulation zone in the 500 m fluid more effectively traps the longer modes than does the deeper fluid. We have offered a simple explanation for this phenomenon. As the group and phase speeds of the Rossby waves increase moderately with the equivalent depth of the fluid (see Fig. 6, WC), the very longest waves will approach the negative stretching region with a slower westward speed as the equivalent depth decreases. As explained by WC, only those modes with a very fast westward translation can escape zeros in their group speeds. Thus, the slower longer modes in the shallower fluid are now trapped.

(iv) The maximum differences in the linear and nonlinear responses for the range of equivalent depth considered, occurred in the accumulation zone itself. Most of the differences (see the bottom panels of Fig. 7) appear to be understandable in terms of the phase differences of linear and nonlinear waves propagating along the equator. This observation appears to be consistent with Simmons (1982), Simmons et al. (1983), Branstator (1985) and Hendon (1986). Elsewhere

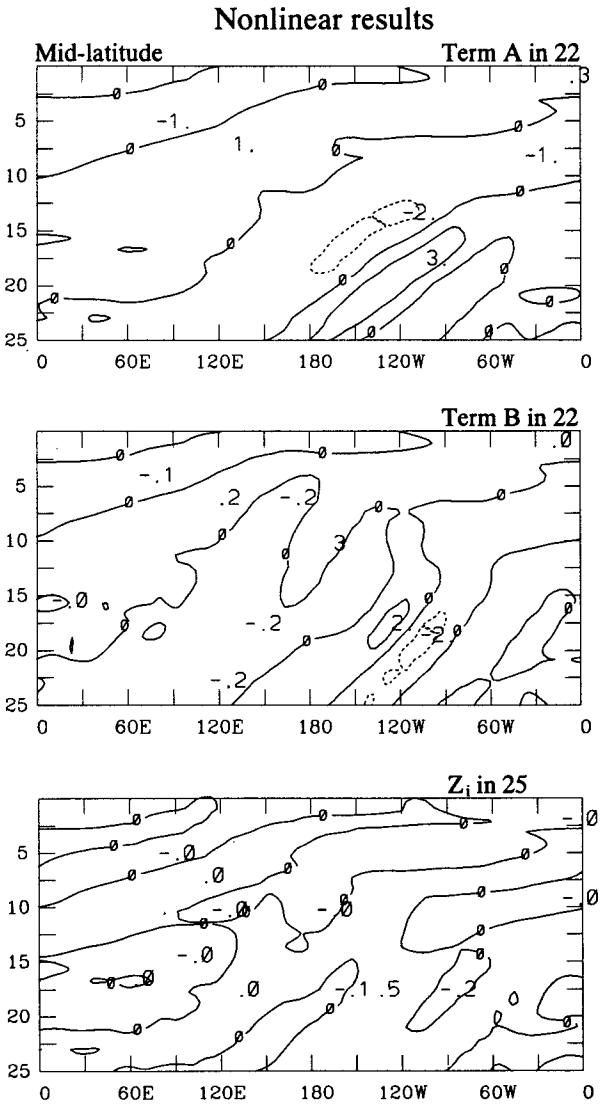

FIG. 12. Diagnostics of the nonlinear height or continuity equation as a function of time and longitude averaged 30°N and 40°N (units: 10^{-5} s^{-1}). Terms are described in the text.

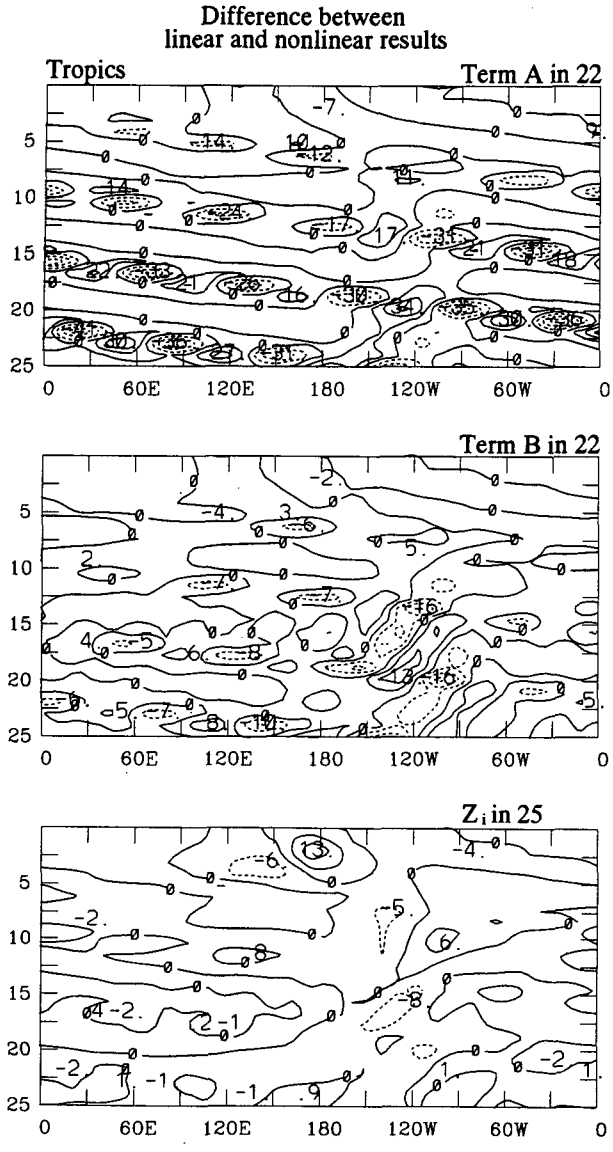

FIG. 13. Diagnostics of the height or continuity difference equation as a function of time and longitude averaged between the equator and 10°N (units: 10^{-6} s^{-1}). Terms are described in the text.

along the equator, there is very little difference in the response. Given the similarity of the linear and nonlinear results, it is not entirely surprising that many of the very large scale characteristics of a GCM can be simulated by much simpler models if the full variation of the basic state is taken into account (e.g., O'Lenic et al. 1985; Branstator 1985).

(v) From a careful examination of Figs. 8a and 8c, it can be seen that nonlinearities only appear in the extratropics after a number of days and then only directly poleward of the equatorial accumulation zone. The inference is that the extratropical nonlinearity originates in the tropics.

(vi) The diagnosis of the linear results (see Figs. 7 and 9–14) indicates that linear advective processes in the tropical regions are very important in the zonal wind balance owing to the nonuniformity of the basic wind field. However, linear advection only plays a secondary role in the extratropics where the forced response is nearly in geostrophic balance. For the meridional wind component, the linear advection is also of secondary importance. In the continuity equation, the largest term is the perturbation divergence associated with the domain averaged height [i.e., $H_{00}(\partial u_l/\partial x) + (\partial v_l/\partial y)$] with the position of maximum amplitude shifting with time to the accumulation region. At this stage, linear height advection becomes an im-

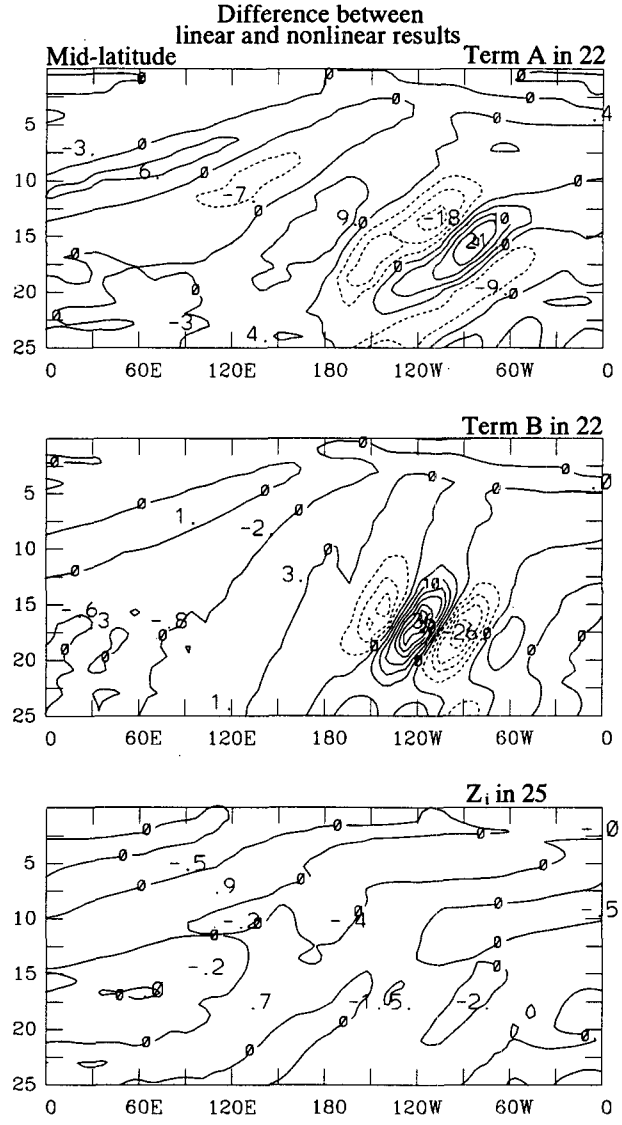

FIG. 14. Diagnostics of the height or continuity difference equation as a function of time and longitude averaged between 30°N and 40°N (units: 10^{-6} s^{-1}). Terms are described in the text.

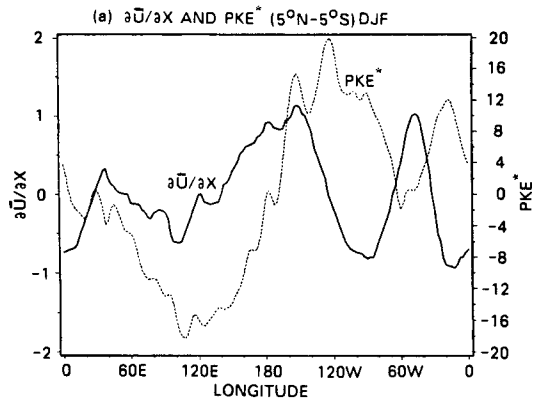

FIG. 15. Longitudinal variability of the longitudinal stretching deformation (U_x: solid line) of the basic flow and the deviation of the perturbation kinetic energy from the zonal average (PKE^*: dashed line) in the latitude band 5°N–5°S for the boreal winter.

portant factor. Clearly, even in the linear regime, the impact of a latitudinally and longitudinally varying basic state will cause large variations in the transient response, especially in the tropics. Thus, the use of models with motionless basic states (e.g., Matsuno 1966, or Gill 1980) or with a basic state containing only latitudinal shear for anything but for the response of the atmosphere to time independent forcing may only produce limited results.

(vii) The diagnosis of the nonlinear results (see Figs. 9–14) showed that the nonlinear advections are of the same order of magnitude as the linear advections. As with the linear advections, the nonlinear advections are much more important in the tropics than in the extratropics. In the nonlinear calculations, the largest term is the pressure gradient term which is compensated somewhat by the nonlinear advection. Examination of the mass field shows that, in the tropics, the nonlinear interaction between the perturbation velocity and the mass fields is a dominant term, especially early in the integration. At higher latitudes, the importance of the nonlinear terms diminish in importance. Thus, in the model calculations, most of the nonlinear modifications are created first by nonlinear interactions between the perturbation mass and velocity fields and the divergence associated with u_d, v_d, and H_{00} in the tropical regions and in the accumulation zones, in particular.

b. Uncertainties and extensions

The results from this study and also from WC point towards some particular problems that need attention. In particular, we are most concerned with the role of stretching deformations at higher latitudes. Are Rossby waves affected in a similar fashion by the basic state as those in higher latitudes? Also, what is the role of the fast teleconnections in the longer term interannual variability of climate? Do the fast teleconnections aggregate to cause longer term climate changes or are they "passive passengers" along conduits determined by the slowly modified basic states involved in the interannual variability?

1) RELATIVE ROLES OF STRETCHING DEFORMATION IN THE TROPICS AND THE EXTRATROPICS

The model results indicate that advective processes only play a minor role in the extratropics. However, this conclusion may be misleading owing to the distribution of our idealized mean state shown in Fig. 7. In our mean field, the mean-flow stretching deformation in the tropics is much stronger than in the midlatitudes. Webster and Chang (see their Fig. 3) showed that the extratropical stretching deformation was at least as large as the tropical values. The motivation for the choice of the basic field in this study was the need to emphasize the tropical flow characteristics as best as possible and to isolate tropical phenomena. However, this does not mean that stretching deformation at higher latitudes is not unimportant. In fact, Farrell and Watterson (1985) have illustrated that the stretching deformation was important for extratropical cyclogenesis and wave propagation. Thus, to determine the real importance of advection in the middle latitudes, an observed mean climate state must be used, or at least, a basic state that more honestly mimics the observed flow at higher latitudes.

2) THE ROLE OF "FAST TELECONNECTIONS" IN THE INTERANNUAL VARIABILITY OF CLIMATE

Recently, Sardeshmukh and Hoskins (1988) investigated the distribution of global rotational flow forced by a specified divergence source in a steady state tropics. Their emphasis was on the long-term mean anomaly flow associated with interannual variability as distinct from the transient modes discussed in this study. They found that the basic characteristics of linear and nonlinear results are the same and that the advection of vorticity by the divergent component of the wind is very important in determining the slow teleconnection patterns between the tropics and the extratropics. To some extent, even with the large difference in time scales, these two results coincide with the conclusions that emerge from sections 5 and 6. We note, though, that the divergence fields in our model are prognostic in contrast to the specified values of Sardeshmukh and Hoskins.

Many of the earlier studies (e.g., Webster 1981, 1982; Hoskins and Karoly 1981; Opsteegh and van den Dool 1980) dealt with the steady state response of a zonally symmetric atmosphere to variations in stationary forcing. The aim was to model the consistent climate state relative to different imposed boundary conditions. All

of these studies found, to one degree or another, dramatic differences to (say) the displacement of anomalous sea surface temperature anomalies or specified convective heating in the tropics. In the study here, we have come to two conclusions. The first is that the basic flow determines almost entirely the regions of accumulation and emanation and, thus, the corridors of propagation through which the transients may influence the higher latitudes. The second is that the linear and nonlinear results, within a very realistic parameter range, of both the basic state and the forcing function are quite similar.

The two principal conclusions of the study allow us to make specific inferences regarding the zero-order role of accumulating and emanating transients in the processes determining the interannual variability of climate. Clearly, such ducted transients have the potential for some importance in connecting the tropics and higher latitudes on the time scales of days to weeks. However, because of their linear nature within realistic parameter ranges, the fast teleconnections would need to have little direct influence on the slowly evolving basic state. The basic state, on the other hand, which is probably the function of a slowly evolving coupled ocean–atmosphere interaction, provides different ducts, or ports, from which transient equatorial influence may emerge towards higher latitudes.

Examples of the changes of the basic state as a function of the time of year and as a function of the sign of the Southern Oscillation Index (SOI) corresponding to El Niño (SOI $\ll 0$) and La Niña (SOI $\gg 0$) for the boreal winter are shown in Fig. 16. The DJF and JJA sections show a considerable difference in the stretching deformation along the equator. In DJF, maxima in U_x exist in the east Pacific and the Atlantic oceans. A secondary maximum exists over the Indian Ocean. Depending on the strength of the westerly winds poleward of the negative U_x regions, these regions may also be emanation regions to higher latitudes for the equatorial transients. In JJA, we might expect there to be minimal accumulation and emanation as the stretching deformation regions are particularly weak.

Between January 1982 and January 1983, the basic wind along the equator changes substantially. During an El Niño event the maximum negative stretching deformation regions and maximum westerlies line over the Atlantic Ocean. During the La Niña period the largest accumulation region (Fig. 16d) lies over the

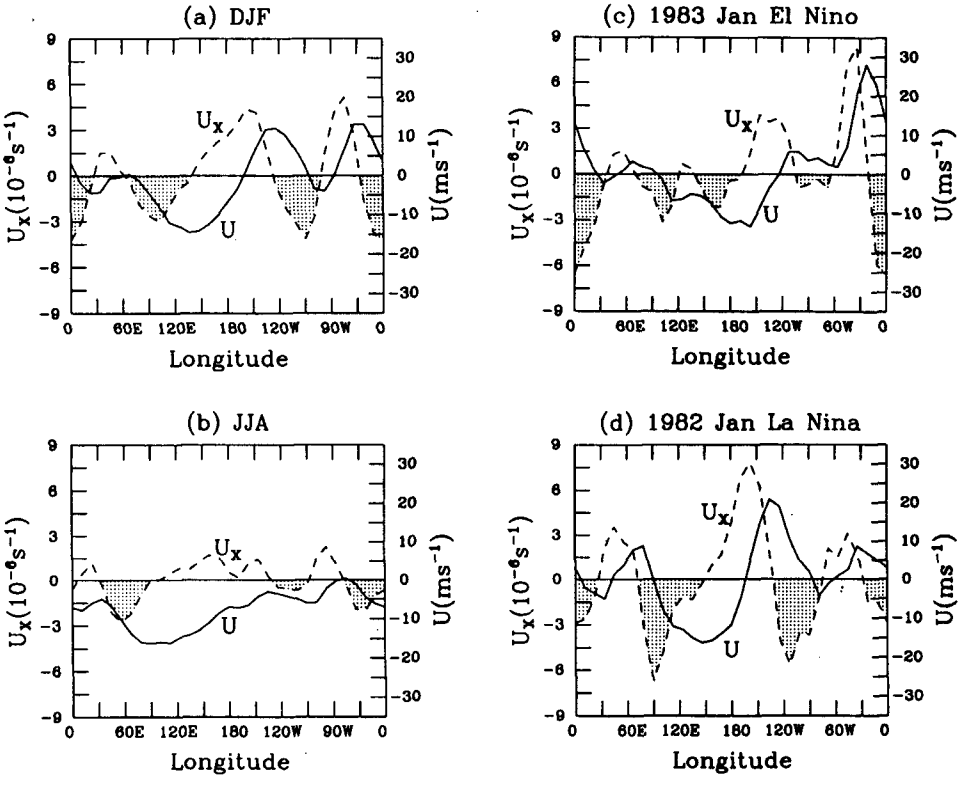

FIG. 16. Variation of the mean basic flow (U: m s^{-1}, solid lines) and the longitudinal stretching deformation (U_x: s^{-1}, dashed lines) along the equator for (a) the long-term mean boreal winter (DJF), (b) the long-term mean boreal summer (JJA), (c) the boreal winter of SOI $\ll 0$ (i.e., El Niño), and (d), the boreal winter of SOI $\gg 0$ (i.e., La Niña). Regions of negative stretching deformation are shaded.

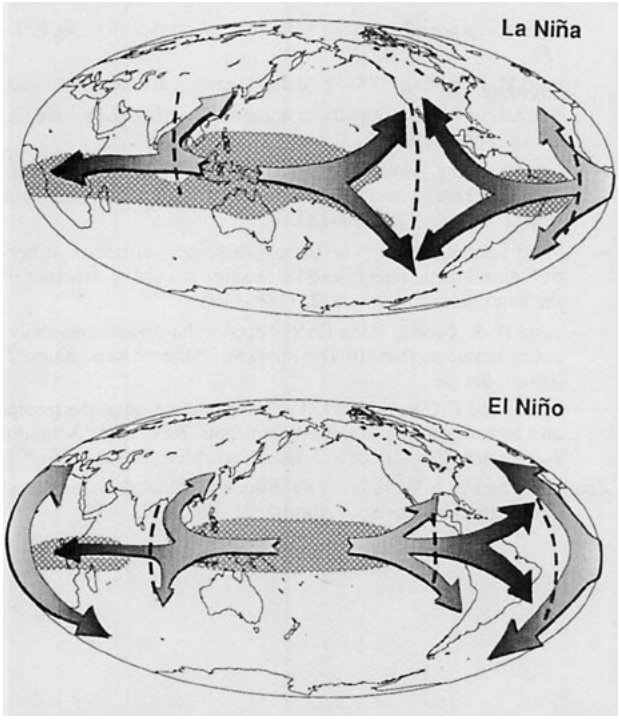

FIG. 17. Schematic diagram showing the impact of different basic states shown in Fig. 16 on the locations of the emanations to higher latitudes. The two panels show basic states similar to La Niña and El Niño situations. The broad arrows indicate regions of transient accumulation along the equator and transient emanation towards higher latitudes. The shaded regions refer to the equatorial easterlies that change substantially in location and intensity, thus varying the stretching deformation along the equator, between extremes in the ENSO cycle.

eastern Pacific Ocean. If the equatorial transients are as sensitive to the basic state as they appear to be from this study, then we would expect a very significant difference between the accumulation and emanation zones for equatorial transients during these phases of ENSO. Schematic views of the longitudinal distribution of the accumulation and emanation zones that may exist for basic corresponding to opposite phases of the ENSO phenomena (i.e., for the SOI $\ll 0$ and $\gg 0$) are presented in Fig. 17. Results from models using these more realistic mean states will be reported in the near future (Webster and Chang 1990).

Acknowledgments. This research was supported by the Atmospheric Sciences Division of the National Science Foundation under Grant ATM 87-03267. We would like to acknowledge Dr. Chidong Zhang for many interesting discussions. The National Center for Atmospheric Research (NCAR) provided computing facilities.

REFERENCES

Arkin, P., and B. N. Meisner, 1987: The relationship between large-scale convective rainfall and cloud cover over the western hemisphere during 1982–84. *Mon. Wea. Rev.*, **115,** 51–74.

——, and P. J. Webster, 1985: Annual and interannual variability of the tropical-extratropical interactions: An empirical study. *Mon. Wea. Rev.*, **113,** 1510–1523.

Branstator, G. W., 1985: Analysis of general circulation model sea-surface temperature anomaly simulations using a linear model. Part I: Forced solutions. *J. Atmos. Sci.*, **42,** 2225–2241.

Boyd, J. P., 1980: Equatorial solitary waves. Part 1: Rossby solutions, *J. Phys. Oceanogr.*, **10,** 1699–1717.

——, 1983: Equatorial solitary waves. Part 2: Envelope solutions. *J. Phys. Oceanogr.*, **13,** 428–449.

Farrell, B., and I. Watterson, 1985: Rossby waves in opposing currents. *J. Atmos. Sci.*, **42,** 1746–1756.

Frederiksen, J. S., and P. J. Webster, 1988: Alternative theories of atmospheric teleconnections and low-frequency fluctuations. *Rev. Geophys.*, **26,** 459–494.

Gelaro, R., 1989: The structure and dynamics of tropical–midlatitude interactions. PhD. thesis, Pennsylvania State University, 228 pp.

Gill, A., 1980: Some simple solutions for heat-induced tropical circulations. *Quart. J. Roy. Met. Soc.*, **106,** 447–462.

——, and P. J. Phillips, 1986: Nonlinear effects on heat induced circulation of the tropical atmospheres. *Quart. J. Roy. Meteor. Soc.*, **112,** 69–91.

Hendon, H. H., 1986: The time mean flow and variability in a nonlinear model of the atmosphere with tropical diabatic forcing. *J. Atmos. Sci.*, **43,** 72–88.

Hoskins, B. J., and D. J. Karoly, 1981: The steady linear response of a spherical atmosphere to thermal and orographic forcing. *J. Atmos. Sci.*, **38,** 1179–1196.

Lau, K. M., and T. J. Phillips, 1986: Coherent fluctuations of extratropical geophysical height and tropical convection in intraseasonal time scales. *J. Atmos. Sci.*, **43,** 1164–1181.

——, L. Peng, C. H. Sui and T. Nakazawa, 1989: Dynamics of multiscale interactions associated with the westerly wind bursts, super cloud clusters, 30–60 day oscillations and ENSO. *J. Meteor. Soc. Japan,* **67,** 205–219.

Lim, H., and C.-P. Chang, 1983: Dynamics of teleconnections and Walker Circulations forced by equatorial heating. *J. Atmos. Sci.*, **40,** 1897–1915.

Matsuno, T., 1986: Quasi-geostrophic motions in the equatorial area. *J. Meteor. Soc. Japan,* **44,** 25–42.

Murakami, T., and S. Unninayer, 1977: Atmospheric circulation during December 1970 through February 1971. *Mon. Wea. Rev.*, **105,** 1024–1038.

Motell, C. E., and B. C. Weare, 1987: Estimating tropical pacific rainfall using digital satellite data. *J. Climate Appl. Meteor.*, **26,** 1436–1446.

Nakazawa, T., 1988: Tropical super-clusters under intraseasonal variation, Japan–US Workshop on the ENSO Phenomena. Meteorological Research Report, #88-1, Department of Meteorology, Geophysical Institute, University of Tokyo, 76–78.

O'Lenic, E., P. J. Webster and A. N. Samel, 1985: The effect of initial uncertainty in tropical analysis upon five day forecasts with NMC's global spectral models. NMC Technical Note No. 311.

Opsteegh, J. D., and H. M. van den Dool, 1980: Seasonal difference in the stationary response of a linearized primitive equation model: prospects for long range weather forecasting? *J. Atmos. Sci.*, **37,** 2169–2185.

Samel, A. N., 1987: The global atmospheric response to isolated tropical forcings in a National Meteorological Center Numerical Weather Prediction Model. MS. thesis, Dept. of Meteorology, Pennsylvania State University, 129 pp.

Sardeshmukh, P. D., and B. J. Hoskins, 1985: Vorticity balances in the tropics during 1982–1983 El Niño Southern Oscillation event. *Quart. J. Roy. Meteor. Soc.*, **111,** 261–278.

——, and ——, 1988: The generation of global rotational flow by steady idealized tropical divergence. *J. Atmos. Sci.*, **45,** 1228–1251.

Simmons, A. J., 1982: The forcing of stationary wave motion by

tropical diabatic heating. *Quart. J. Roy. Meteor. Soc.*, **108,** 503–534.

——, J. M. Wallace and G. W. Branstator, 1983: Barotropic wave propagation and instability, and atmospheric teleconnection patterns. *J. Atmos. Sci.*, **40,** 1363–1392.

Taylor, R., 1973: *An Atlas of Pacific Rainfall, HIG-73-9.* Hawaii Institute of Geophysics, 7 p.

Van Tuyl, A. H., 1986: Advective influences enforced tropical motions. *J. Atmos. Sci.*, **43,** 141–161.

——, 1987: Nonlinearity in low-frequency equatorial waves. *J. Atmos. Sci.*, **44,** 2478–2492.

Webster, P. J., 1972: Response of the tropical atmosphere to local steady forcing. *Mon. Wea. Rev.*, **100,** 518–540.

——, 1981: Mechanisms determining the atmospheric response to sea surface temperature anomalies. *J. Atmos. Sci.*, **38,** 554–571.

——, 1982: Seasonality in the local and remote response to sea surface temperature anomalies. *J. Atmos. Sci.*, **39,** 41–52.

——, 1983: The large-scale structure of the tropical atmosphere. *Large-Scale Dynamical Processes in the Atmosphere,* B. Hoskins and R. Pearce, Eds., Academic Press, 235–276.

——, and J. R. Holton, 1982: Cross equatorial response to midlatitude forcing in a zonally varying basic state. *J. Atmos. Sci.*, **39,** 722–733.

——, and H. R. Chang, 1988: Equatorial energy accumulation and emanation regions: Impact of a zonally varying basic state. *J. Atmos. Sci.*, **45,** 803–829.

——, and S. Yang, 1989: The three-dimensional structure of perturbation kinetic energy and its relationship to the zonal wind field. *J. Climate,* **2,** 1210–1222.

——, and S. Yang, 1989: The three-dimensional structure of perturbation kinetic energy and its relationship to the structure of the wind field. *J. Climate,* **2,** 1186–1198.

——, and H.-R. Chang, 1990: Energy accumulation and emanation at low latitudes. Part III: The impact of different basic states. *J. Atmos. Sci.*

——, —— and C. Zhang, 1989: The joint interaction of the tropics and higher latitudes: some new concepts. *Proc. of the Southern Hemisphere Conf.,* Buenos Aires. Amer. Meteor. Soc., 386–392.

Zhang, C., and P. J. Webster, 1989: Effects of zonal flows on equatorially trapped waves. *J. Atmos. Sci.*, **46,** 3632–3652.